# Green synthesis process for catalytic zeolite materials

# ゼオライト触媒材料のグリーン合成

**Xu Sun**

**孫 旭**

Supervisor: Prof. Noritatsu Tsubaki

Tsubaki Laboratory

Graduate School of Science and Engineering

University of Toyama

# Preface

Zeolite was first discovered in 1756. Axel Fredrik Cronstedt, a Swedish mineralogist, found that a type of natural aluminate silicate ore will boil when burning, so it was named "zeolite" (Swedish zeolites). Zeolites can be divided into natural zeolite and artificial zeolite. More than 80 kinds of natural zeolite have been found all over the world, among which clinoptilolite, mordenite, chabazite, erionite, and analcime are the most common. Clinoptilolite and mordenite have been widely used. Zeolite minerals belong to different crystal systems, with most crystals appearing in fibrous, hairy, or columnar shapes. The general chemical formula of zeolite is: $AmB_pO_{2p} \bullet nH_2O$, the structural formula is $A_{(x/p)}$ $[(AlO_2)_x$ $(SiO_2)_y] \bullet n(H_2O)$ where A is cations such as Ca, Na, K, Ba, Sr, B is Al and Si, p is the valence of cations, m is the number of cations, n is the number of water molecules, x is the number of Al atoms, y is the number of Si atoms, (y/x) is usually between 1 and 5, and (x+y) is the number of tetrahedrons in the unit cell.

Afterwards, people's research on zeolite continued to deepen. In 1932, McBain proposed the concept of "molecular sieve". A classic porous material that can screen substances at the molecular level. Up to now, there are over 200 artificially synthesized zeolites included in the zeolite data basement. Zeolite materials have good ion exchange properties, adsorption and separation properties, thermal stability, chemical reactivity, reversible dehydration, conductivity, etc. It is widely used in fields such as petrochemical, environmental, and gas separation. Zeolites are often used as catalytic carrier materials in the field of C1 chemistry. Because zeolites have unique acid centers that enable secondary reactions such as cracking, polymerization, and isomerization of products. At the same time, the selectivity effect of the pores in zeolites can effectively screen the target product, which can regulate the selectivity of C1 products, thereby achieving the goal of high selectivity and high yield of products.

The development process of zeolite has been going on for a long time now. The commonly used methods of small-scale synthesis in laboratory include solvothermal

method (hydrothermal method), dry gel method, ultrasonic synthesis and microwave synthesis. The commonly used large-scale method in industry is solvothermal method, which uses liquids such as water and ethanol as solvents to industrially synthesize zeolite under high temperature and pressure conditions. Although this method can achieve advantages such as good product dispersion and uniform morphology. The disadvantage is also obvious, as a large amount of alkaline wastewater is generated during the product purification process, and there is a potential explosion hazard during the production process due to high temperature and pressure. Therefore, how to produce zeolite materials in a green and safe manner is a hot research topic for many scientists.

We were inspired by Chongqing Hot Pot. Oil sealent above the liquid phase layer, which can isolate the external environment and reduce material exchange. In the chapter 1, we used the liquid sealant method to synthesize zeolite under atmospheric pressure. The results showed that LTA (NaA), MFI, FAU and BEA zeolites could be successfully synthesized under atmospheric pressure conditions of 90-120 $^{o}$C. Among them, we used NaA zeolite as a model to explore the conditions of crystallization temperature, crystallization time, type of liquid sealant solution, weight of liquid sealant solution, weight loss, and template in detail. The zeolite was characterized and analyzed by XRD, SEM, TEM, BET, NMR, and UV-Raman, and compared with the parameters of NaA zeolite synthesized by hydrothermal method. The results indicate that the optimal conditions for the synthesis of NaA zeolite are 120 °C and 4 hours.

Due to the severe limitations of temperature and test tube space caused by the liquid sealant method, in order to further optimize the process of synthesizing zeolite at atmospheric pressure, we focused on designing a reflux device that can synthesize zeolite at atmospheric pressure in chapter 2. We explore the synthesis conditions using NaA zeolite as a model. This device can use a reflux device to reduce liquid evaporation and consumption while maintaining ambient pressure and high temperature. The original liquid sealant method for atmospheric pressure synthesis can only be used for small-scale static synthesis of zeolite in test tubes. As a

comparison, the reflux synthesis device can perform large-scale dynamic synthesis. Under dynamic crystallization, the crystallization periods can be shortened, thereby reducing energy consumption.

Solvent-free synthesis method is a green synthesis process of zeolite. During the synthesis process, zeolite can be obtained through simple grinding of raw materials and high-temperature crystallization without adding any solvents. This method can reduce wastewater discharge due to the lack of solvent addition. In chapter 3, we take Silicalite-1 zeolite as an example and use a solvent-free method to rapidly synthesize submicron sized zeolites. We focused on exploring conditions such as crystallization temperature, crystallization time, and raw material ratio. The Silicalite-1 zeolite was characterized and analyzed by XRD, SEM, BET, and UV-Raman. The results indicate that the crystallization of Silicalite-1 zeolite can be successfully synthesized at 180 $^{o}$C for 45 minutes. In addition, replacing the template with tetrabutylammonium hydroxide (TBAOH) and 1,6-hexanediamine can achieve rapid synthesis of Silicalite-2 and ZSM-22 zeolite, respectively. This process not only reduces the discharge of wastewater, but also greatly shortens the crystallization time, thereby reducing energy consumption.

# Contents

# Chapter 1

# Ambient Pressure Synthesis (APS) of Highly Crystallized Zeolite

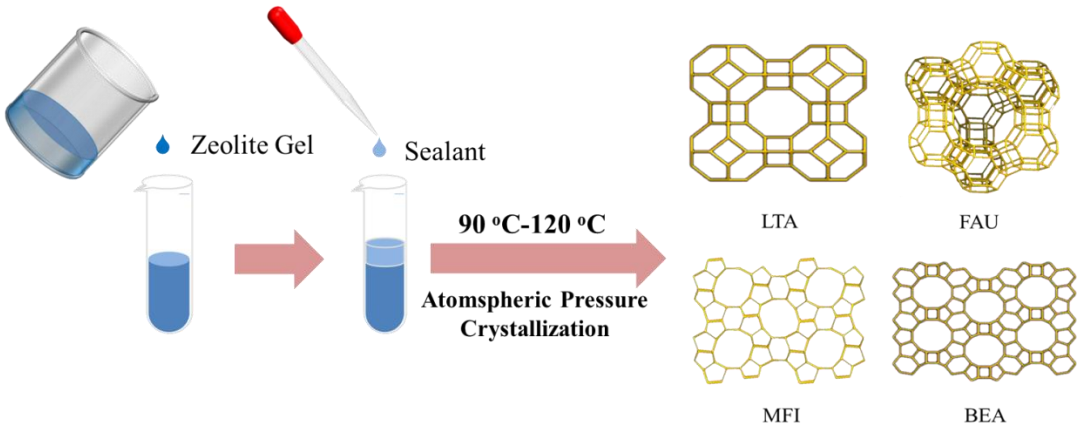


The traditional method for zeolite synthesis is challenged with high operating costs and safety issues. In the chapter 1, we detail the NaA zeolite under an ambient pressure synthesis process. The procedure presented in this work is simple, green, safe, and cost-effective when compared with the traditional method.

# Abstract

Zeolite's great momentum in industrial applications will require an efficient route for their synthesis. The conventional methods for zeolite synthesis normally involve expensive reactor set-ups while the crystallization occurs at high-pressure conditions. Herein, we proposed an ambient pressure synthesis (APS) of NaA zeolite at 120 °C. The reaction setup simply used a glass tube as a reactor and a low-density liquid as a sealant. The optimum synthesis conditions were achieved by a methylcellulose template and PEG-400 sealant. Compared with the conventional hydrothermal process, the barrier of sealant over the zeolite gel in the glass tube can significantly reduce the synthesis cost, but also makes the process much safer than the conventional methods.

**Keywords：** LTA, Zeolite, Ambient pressure synthesis, Sealant.

## 1.1 Introduction

Zeolites, composed of tetrahedrons of silica and alumina linked to each other by oxygen atoms, offer structures with unique pore properties [1-3], molecular selectivity [4], ion-exchange capacity [5], and high chemical and thermal stability [6]. Low-cost synthesis and easy modifications can widen their scope of industrial applications such as in catalysis, separation, and medicine [7-11]. Zeolites can occur naturally or can be synthesized from reagents [12]. The synthetic zeolites are industrially preferred as further purification steps are not needed and have uniformity in structures and pore size [13, 14].

There is an increasing job of literature about the different methods, which have been employed for the synthesis of zeolites with unique and specific application properties [15-18]. Nevertheless, it is a tedious job to produce a zeolite of desired crystallinity, anticipated framework topology, and porosity for better application at a low production cost. Conventionally, zeolites are produced from high-pressure hydrothermal synthesis in an autoclave [19, 20]. The consequences of using this method are to have safety concerns of high reaction pressure, environmental pollution due to wastewater, large requirements on energy, and Teflon reactors [21]. The wastewater issue has been minimized in the dry gel conversion (DGC) method, however, this strategy has elevated temperature and pressure challenges since crystallization occurs in an autoclave sealed reactor [22]. Interestingly, the solvent-free method is consisted of manually grinding the raw materials, and crystallizing the material without adding additional water or solvents [23]. This solvent-free method not only omits the step of solvent vaporization to obtain the dry gel as in the DGC method but also reduces the wastes. Nonetheless, crystallization still proceeds in sealed vessels at elevated pressure, and safety concern remains there. Development of green synthesis processes has thus become an important issue for the zeolite synthesis [24]. Deborath et. al. proposed a route of NaY

synthesis through an ultrasonic assisted aging at low temperature with elevated surface area ($S_{BET} \sim 950\ m^2\ g^{-1}$) and hierarchical micropores and mesopores with X~0.4 $cm^3\ g^{-1}$ pore diameter [25]. Pal et al. successfully synthesize zeolite NaP crystals with low crystallinity at room temperature and reduced pressure by sonochemical method. It was also investigated that, by increasing the ultrasonic radiation energy and time, the crystallinity of NaP zeolite can be improved a little [26]. More recently, Zhang and co-workers synthesize Silicalite-1 from fumed silica with a crystal size of 150 nm and high BET surface area (466 $m^2/g$) at ambient pressure and 90 $^oC$ without waste discharge [27].

Particularly, Linde-A (LTA) zeolite has most widely used due to its high cation exchange capacity concomitant with its high Al content [28, 29]. The easy ion exchangeable nature of Na with Ca and K provides NaA zeolite diversity in pore opening, and hence make NaA the most synthesized zeolite worldwide [30, 31]. The largest industrial application of zeolite LTA is in the detergents builder and water softener composition [32, 33]. Thiago et al. used coal fly ash as a source of Si and Al with NaOH for the synthesis of LTA zeolite and managed to produce 70% crystalline zeolite type through alkaline fusion treatment followed by hydrothermal process [34].

Herein, we introduce a facile ambient pressure synthesis (APS) of zeolite NaA crystals. In this tactic, the reaction occurs at ambient pressure and 120 $^oC$ temperature in a glass tube, as an oil sealant is used in place of the Teflon reactor to create a physical barrier between the raw material content and the surroundings. The technique is employed with different kinds of sealants to see their effect on the crystallinity of NaA zeolite. Also, the crystallization environment is optimized by varying the temperature, water content in gel, sealant type, and amount in the NaA crystallization process. Moreover, methylcellulose (MC) templates with different amounts are also used in the APS procedure to improve the pore properties of NaA zeolite. A systematic

comparison of conventional hydrothermal process and proposed APS has also been discussed, winding up the APS is a highly efficient, safe, and low-cost zeolite synthesis process.

## 1.2 Experimental Section

### 1.2.1. Materials

$NaAlO_2$, NaOH, $Na_2SiO_3 \cdot 9H_2O$ (Sinopharm Chemical Reagent Co. Ltd.), Methylcellulose (MC, Aladdin Industrial Corporation), Polyethylene glycol (PEG-400) and Polyethylene glycol (PEG 6000, Qingdao Yusuo Chemical Technology Co. Ltd.), Silicone oil (Zhejiang Rongcheng Organic Silicon Material Co. Ltd. boiling point 250 $^oC$), 1-Dodecanol (Shanghai Macklin Biochemical Co. Ltd.), Glycol (Hangzhou Gao Jing Fine Chemical Co. Ltd.) Ethylene glycol (Shanghai Lingfeng Chemical Reagent Co. Ltd.) and deionized water were used in the synthesis of NaA zeolite. All the materials were used without further purification.

### 1.2.2 Zeolite Synthesis

A method was reported for zeolite NaA synthesis. In a typical run, two gels (seed and feedstock) were prepared. Initially, two solutions were prepared with the same composition by adding 8 g $H_2O$ and 0.115 g NaOH under vigorous stirring into a beaker. Later, 2.2 g $Na_2SiO_3 \cdot 9H_2O$ was added in one of the solutions and named as seed gel, and the other 1 g $NaAlO_2$ to prepare a feedstock gel. Under continuous and vigorous stirring, the seed gel was slowly added to the feedstock to obtain an overall gel. The overall gel was stirred continuously for 30 min, transferred to a glass tube, and different kinds of sealant were used in the synthesis of zeolite NaA. The overall gel was later put into the laboratory oven and crystallized at 120 $^oC$ for 4 hours. For liquid sealant separation, the top liquid layer (sealing liquid) was first sucked out with

a rubber tipped dropper. After washing with 1-1.5 ml of toluene three times, the sample was further washed with deionized water to ensure complete separation. Lastly, it was dried overnight at 90 $^{o}$C to get the final form of NaA zeolite. The synthesis process of NaA zeolite was repeated at different temperatures (90-130 $^{o}$C), with different sealants (Silicon oil, PEG-400, without seal, Dodecanol, Ethylene glycol, and Glycol), with different amounts (4-16 g) of water in alkaline solution, and samples were also prepared by varying the amounts (0-6.0 g) of silicon oil sealant. Several samples were also prepared to MC template was added in the feedstock gel and later this mixture of feedstock and MC was gradually added to the seed gel and mixed well to get the final gel of NaA zeolite and after following the same procedure to get the final NaA zeolite crystals.

## 1.2.3 Zeolite Characterization

X-ray diffractions (XRD) of as-prepared samples were performed on a Rigaku Ultima IV diffractometer with Cu Kα radiation basis and data collected in 2θ = 5-50° (λ=1.54 Å, scanning rate of 4°/min at 40 kV and 20 mA). The morphologies of the synthesized zeolite were investigated with Scanning Electron Microscopy (SEM) and images of all samples were obtained on a Hitachi SU1510. Transmission Electron Microscopy (TEM) images were achieved on a FEI Tecnai F20 microscope at 200 kV. The textural properties of the samples were measured by $N_2$-physisorption on a Micromeritics ASAP2460. In the pretreatment step, 2 g NaA zeolite sample was dissolved and stirred in 70 mL of $Ca(NO_3)_2$ solution in a hot water bath at 60 $^{o}$C for an hour, the sample was then washed, dried at 120 $^{o}$C and calcined at 400 $^{o}$C for 4 hours. The surface area of CaA samples was calculated from the Brunauer-Emmett-Teller (BET) equation whereas the pore sizes were determined by the Barrett-Joyner-Halenda (BJH) method. Thermogravimetry analysis (TGA) differential scanning calorimetry was achieved with a Netzsch STA449F3 analyzer. $^{27}$Al and $^{29}$Si NMR spectra were employed on a Bruker Avance IIITM

at 400 MHz. UV-Raman spectra were measured with a LabRAM HR Evolution with a spectral resolution of 2 $cm^{-1}$.

## 1.3 Results and Discussion

### 1.3.1 Effect of water content on NaA crystallization

Water content has a significant role in the formation of LTA zeolite crystals as the water to silica ratio controls the rate of nucleation and hence the crystal growth. Figure 1.1 shows the zeolite NaA crystallization with various water content in the APS method for zeolite NaA synthesis at 120 °C with $SiO_2/Al_2O_3/Na_2O$=1.9:1.3:1.6 and silicon oil as a sealant. XRD patterns in Figure 1.1a show that there is an enhancement in crystallization with increasing water content in the gel solution from 4 to 8 g. This is due to the fact that water content improved the diffusion of substrates and helped in the free migration of silicate intermediate species. However, further increment in water amount to 12 and 16 g, diluted the solution and lower down the concentration of primary species which resultantly reduced the crystallization rate. A large amount of water decreased the crystallinity of NaA zeolite as compared to 8 g, but still, have the higher crystallinity as compared to commercial NaA (Figure 1.1b).

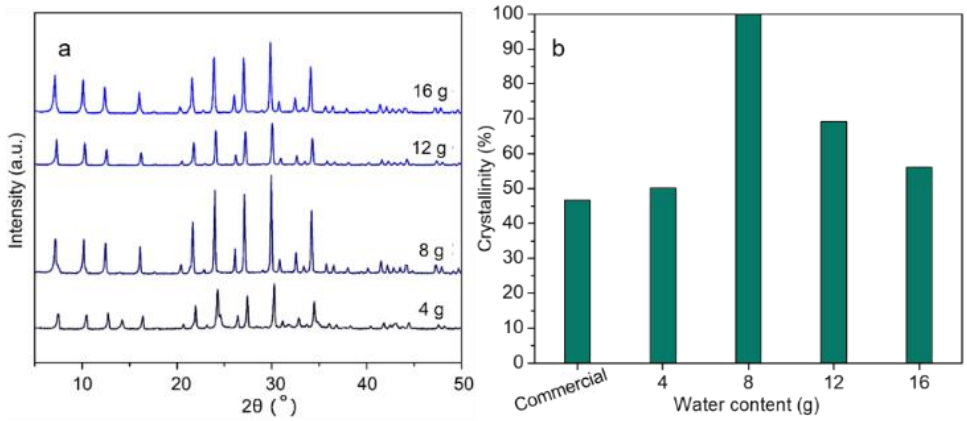


**Figure 1.1.** (a) XRD peaks of NaA crystals (b) impact of water content on NaA zeolite crystalization, synthesize from APS system at 120 °C and varying the

water amount to X g where X=4, 8, 12, and 16 in samples with $SiO_2/Al_2O_3/Na_2O$=1.9:1.3:1.6 and 0.3 g silicon oil as a sealant and commercially prepared NaA zeolite.

## 1.3.2. Effect of temperature on NaA crystallization

Figure 1.2 shows the zeolite NaA crystallization at different temperatures with various water content in the APS synthesis of zeolite NaA. The XRD patterns presented in Figure 1.2 indicate that the crystallization of zeolite NaA is temperature-dependent. The diffractograms show that when crystallization is performed at 80 $^oC$, XRD peaks are very small in the case of 8 and 12 g water content, and only amorphous phases are observed for 16 g water in the gel. XRD peak strength increased with increasing temperature for all the water content (Figure 1.2a-c), as the rise in temperature increased the average particle size of the crystals. However, when the crystallization temperature is extended to 120 $^oC$, perfect diffraction peaks depicting the successful synthesis of zeolite with LTA topology. At 130 $^oC$ prominent typical LTA peaks are still observed but not as significant as those at 120 $^oC$. These results suggest that highly crystallized zeolite NaA is achieved at 120 $^oC$ with 8 g of water under the selected synthesis conditions. Figure 1.2d shows the relationship between the crystallinity of zeolitic materials and variation in temperature and water content in the gel solution.

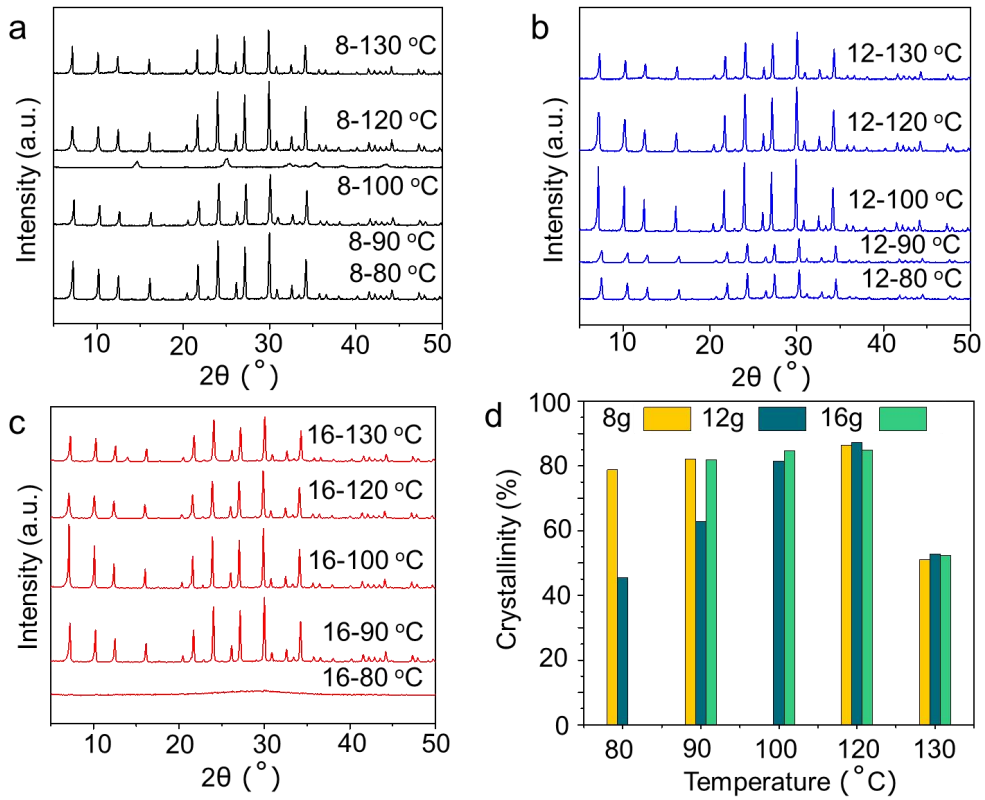


**Figure 1.2.** XRD patterns at for (a) 8 g, (b) 12 g, (c) 16 g water, and (d) NaA zeolite crystallinity at different temperatures of 80, 90, 100, 120, and 130 °C with $SiO_2/Al_2O_3/Na_2O$=1.9:1.3:1.6 in an APS system with no sealant oil.

## 1.3.3. Effect of sealant type on NaA crystallization

In an APS system, the edges of the reaction scheme are not fixed henceforth internally built pressure is ousted as the volume of contents increases. To create a pseudo-closed pressure system, a seal is employed as a physical barrier between the glass tube contents and the atmosphere. Liquid sealants act as a barrier between the direct contacts of zeolite gel with environment and also prevent water from volatilizing during heating that resultantly affect the synthetic environment. For the selection of liquid sealant, it is very important to check the physical properties of the sealant at higher temperature i.e. liquid stability, boiling point, solubility and density. Figure 1.3 shows the effect of different sealants on zeolite NaA crystallization. The XRD diffractograms in Figure 1.3a show peaks representing LTA-type zeolite on all

samples treated with different sealants at 120 ºC with 8 g water content under the above reaction conditions. Although all samples display diffraction peaks with LTA topology, peak intensity is different (Figure 1.3a). The differences in peak intensities suggest that the resulting crystallinity depends on the inherent properties of the sealant oils. The NaA zeolite gel sealed with silicon oil showed significant peak intensity compared to the other sealants. Figure 1.3b shows that the dodecanol and PEG-400 are unaffected by the synthesis conditions and are perfectly close off the exchange of matter between the atmosphere and reaction system hence reduced the crystallinity as compared to silicon oil.

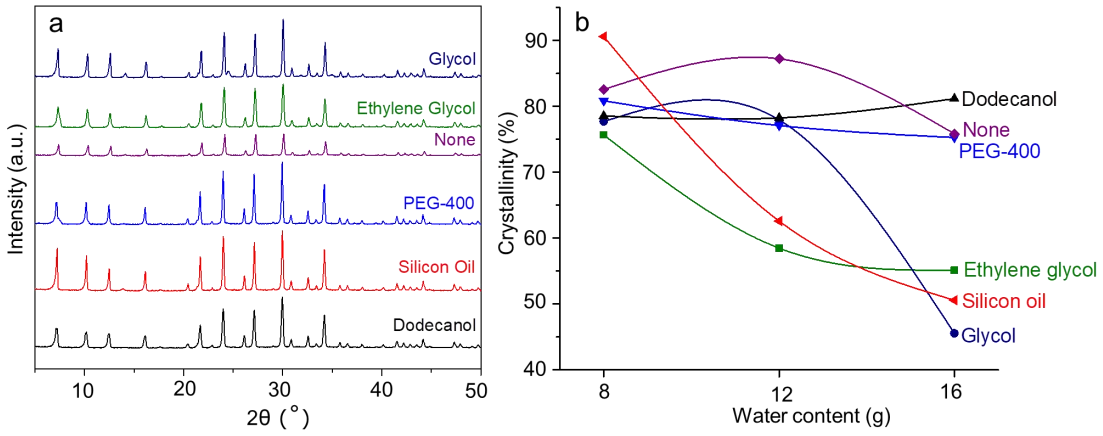


**Figure 1.3.** (a) XRD peaks of NaA zeolite with 8 g water amount in gel (b) NaA zeolite crystals synthesize with 8, 12, and 16 g water amount in gel, in an APS system with $SiO_2/Al_2O_3/Na_2O$=1.9:1.3:1.6 at 120 ºC with 1 g different sealants.

There is a general loss of weight for the samples under investigation over time (Figure 1.4). The non-sealed sample loses more weight compared to the sealed samples because there is less physical hindrance to reducing pervaporation as shown in Figure 1.4. Silicon oil sample loses the least weight because of its high thermal resistance and expansion. Different oil sealants with unique densities possess a different effect on the mass-loss rate and hence on crystallization in each case. The results showed that silicon oil is the optimal

sealant for zeolite NaA synthesis at 120 °C with 8 g of water in the gel.

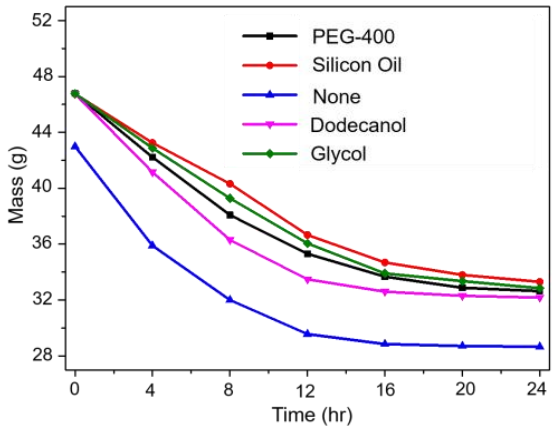


**Figure 1.4.** Mass loss in different gel solutions over time for different sealant oils during NaA crystallization process through an APS system at 120 °C with 1 g different sealants.

## 1.3.4. Effect of silicon oil sealant content on NaA crystallization

Figure 1.5a exhibited the silicon oil sealant content effect on crystallization of NaA zeolite. Though all the XRD peaks in Figure 1.5a evidenced the formation of NaA crystals, these samples with different silicon oil content possess different peak intensities. Zeolite gel solution with no sealant oil exhibited NaA crystallinity 84% and decreased to 65% when a thin layer (1.5 g) of silicon oil was used. This is might due to the fact that the thin layer of silicon oil not provided the perfect immiscibility in both the phases and impure the zeolite gel. NaA zeolite crystallinity increased to a maximum of 93% with 3.0 g of silicon oil sealant as shown in Figure 1.5b. However, crystals formation drastically reduced when the oil amount was further increased to 4.5 g and 6.0 g. Hence, the amount of 3 g of silicon oil provided the optimum physical barrier in between the zeolite solution gel and the environment.

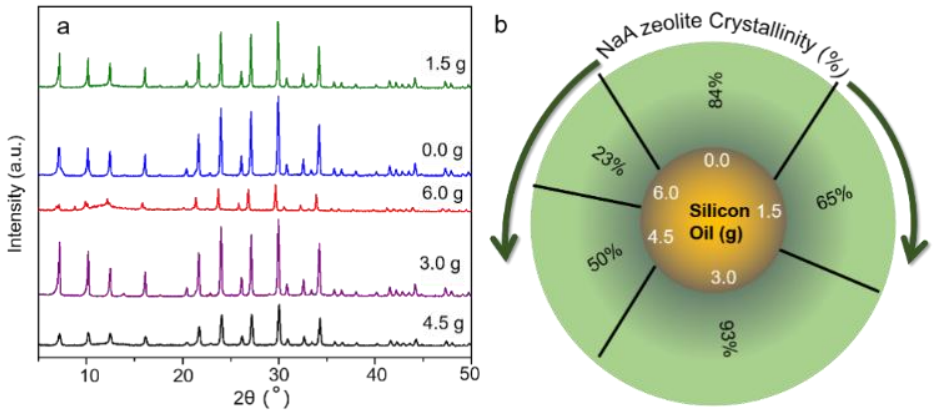


**Figure 1.5.** (a) XRD peaks of zeolite NaA crystals (b) influence of silicon oil sealant amount on NaA zeolite crystallinity, with different oil sealant content at 120 °C with $SiO_2/Al_2O_3/Na_2O$=1.9:1.3:1.6 and 8 g water in NaA zeolite gel.

## 1.3.5. Effect of methyl cellulosic template

Organic templates are employed in the synthesis process to improve porosity, specifically mesopores. Figure 1.6a exhibits the XRD pattern of zeolite NaA in the presence of 30 mg methyl cellulose (MC) template with different sealants at 120 °C, 8 g water in NaA zeolite gel, with $SiO_2/Al_2O_3/Na_2O$=1.9:1.3:1.6 through APS crystallization process. Graphs exhibit that NaA peaks are higher in the case of using PEG-400 oil sealant as compared to other samples with different sealants when using the MC template. As the isotherms indicated high crystallinity for PEG-400>none>silicon oil>dodecanol samples respectively. For selecting the optimized MC amount, XRD was performed for different samples by varying the MC content. Figure 1.6b showed that the APS sample in combination with 30 mg MC has higher XRD peaks as compared to the other samples with different MC amounts. Textural analysis in Figure 1.6c suggested that LTA zeolites in common do not exhibit adsorption isotherm due to the $Na^+$ ion hindrance near the 8 member ring pore [35]. Template has been added to obtain modified NaA zeolite in terms of getting smaller zeolite crystalline particles and to improve the surface area of as prepared zeolite. The experimental results showed that methylcellulose (MC) can modify the pore structure

of NaA zeolite, as shown in Table 1.1, and Figure 1.6c. However, the data revealed that BET surface area increased gradually as the amount of MC template is increased in the zeolite samples. Particularly, the maximum surface area of 844 $m^2/g$ was obtained from 60 mg MC with the higher amount of mesopores volume 0.11 $cm^3/g$. By further increasing the MC amount to 75 mg, the surface area reduced and XRD peaks also decreased. A decreasing trend in zeolite crystallinity clearly suggested that further addition of MC template inhibited the crystallization process (Figure 1.6b).

**Table 1.1** BET surface area and pore volume of zeolite CaA with different MC amount of 15, 30, 45, 60 and 75 mg with $SiO_2/Al_2O_3/Na_2O$=1.9:1.3:1.6 and 8 g water in zeolite NaA gel at 120 °C produced from ambient pressure strategy (APS).

| Samples | MC(mg) | $S_{BET}(m^2/g)^a$ | $V_{meso}(cm^3/g)^b$ | $V_{micro}(cm^3/g)^b$ | $V_{total}(cm^3/g)^b$ |
|---|---|---|---|---|---|
| 15MC | 15 | 279 | 0.03 | 0.13 | 0.16 |
| 30MC | 30 | 525 | 0.06 | 0.22 | 0.28 |
| 45MC | 45 | 647 | 0.08 | 0.27 | 0.35 |
| 60 MC | 60 | 844 | 0.11 | 0.34 | 0.45 |
| 75MC | 75 | 443 | 0.06 | 0.18 | 0.24 |

[a] $S_{BET\ (total\ surface\ area)}$ calculated using the BET equation.

[b] $V_{(total\ pore\ volume)}$ calculated by single-point method at $P/P_0$=0.95.

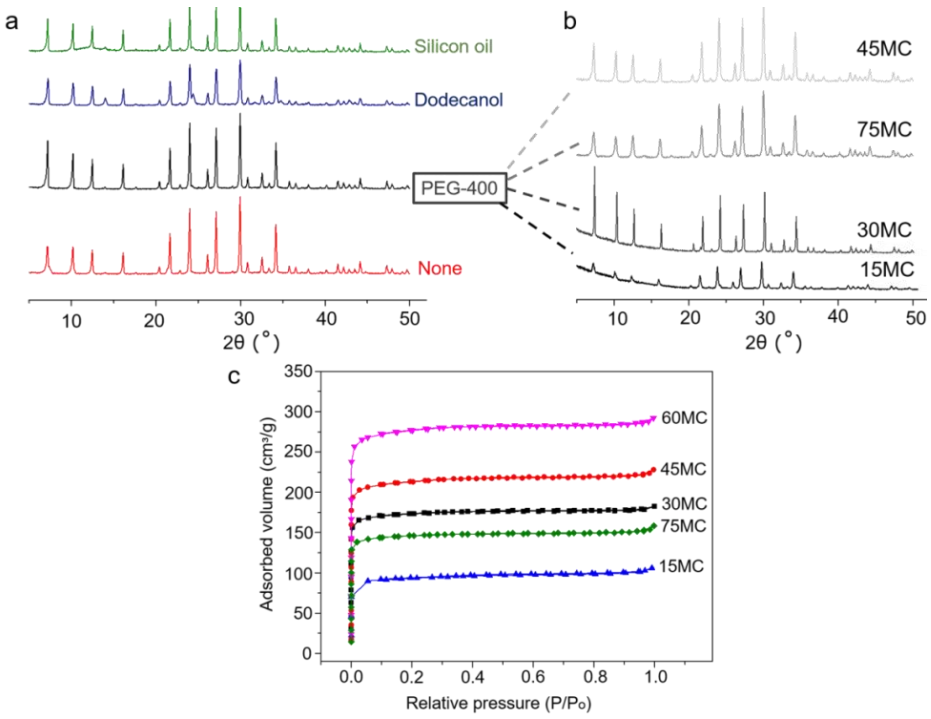

**Figure 1.6.** (a) XRD patterns and of the sample with 0.03 g MC template with different sealants, (b) XRD patterns and of the sample with PEG-400 sealant and different MC amount, (c) $N_2$ physisorption isotherms of zeolite CaA in ambient pressure system (APS) with different MC amount of 15, 30, 45, 60, and 75 mg at 120 $^oC$, and 8 g water in an APS system.

Figure 1.7 shows the TG curves of NaA zeolite samples prepared from APS system with PEG400 sealant, when different MC template amounts of 15, 30, 45, 60, 75 mg was used. The measured weight loss curve is nearly identical for all samples at low temperature upto 200 $^oC$, which represent the loss of moisture in the samples. Weight loss around 600-800 $^oC$ is increasing in each case, which shows the burning of MC carbon. The carbon burning is maximum for the zeolite sample with 75 mg MC, as it can be observed in Figure 1.7e, and this is due to the fact that this sample has maximum MC as compared to other samples.

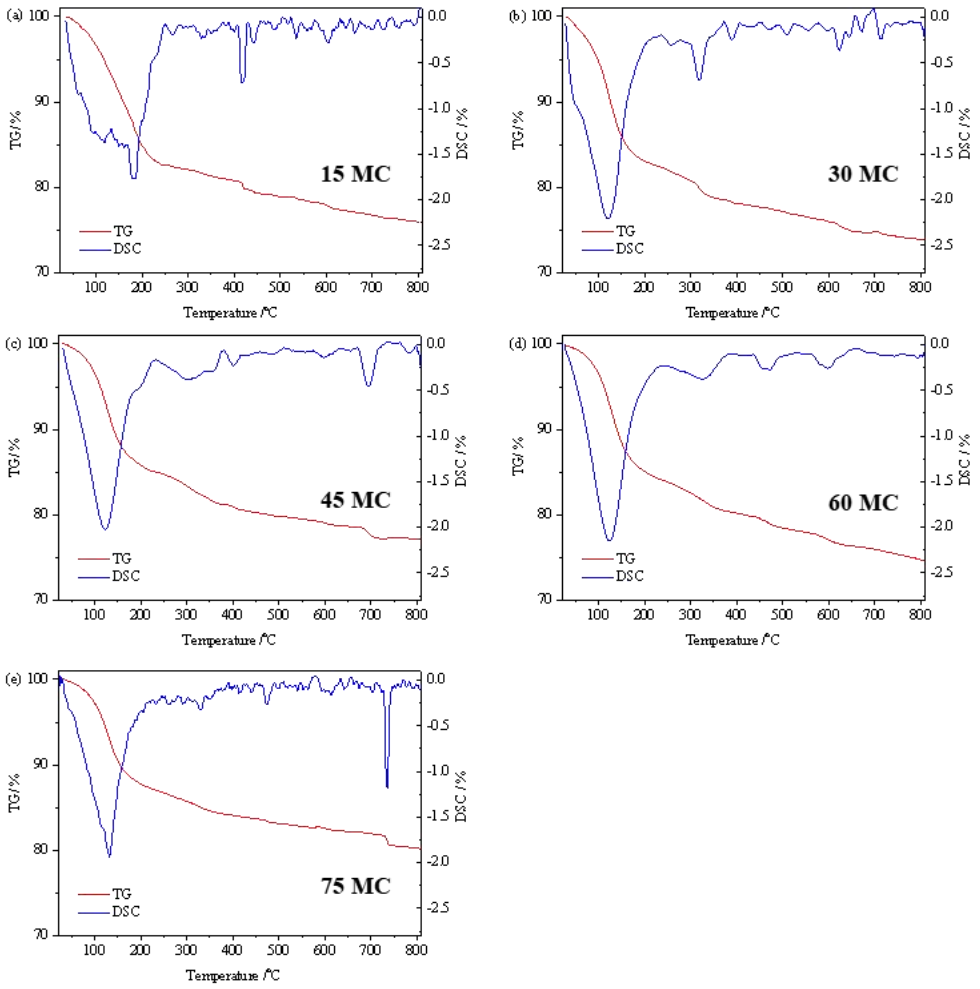


**Figure 1.7.** TG analysis of zeolite NaA with different MC amounts of 15, 30, 45, 60, and 75 mg, at 120 °C, and 8 g water with PEG 400 sealant in an APS system.

## 1.3.6. Effect of system configuration

In the ambient pressure strategy (APS), the zeolite was synthesized in the simplest test tube with oil sealant at 90 °C at normal pressure. In this proposed route, the time and energy being required for achieving complete crystallization were further shortened as compared to HT sample. As indicated by the XRD pattern, both the systems exhibited the successful formation of NaA crystals with the clear SEM image showing cubical LTA topology with no amorphous $SiO_2$ present in there (Figure 1.8). However, the NaA crystals synthesized through the APS route showed greater XRD peak strength as compared to the

conventional HT route.

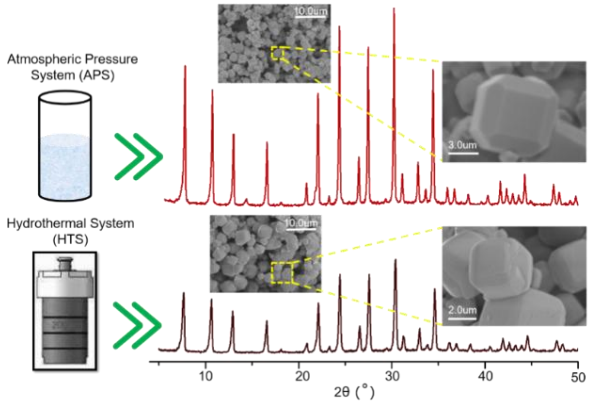


**Figure 1.8.** System comparison of APS system and hydrothermal (HT) process for zeolite NaA synthesis with $SiO_2/Al_2O_3/Na_2O$=1.9:1.3:1.6 at 120 °C for 24 h, and 8 g water in gel.

Figure 1.9 exhibited the TEM micrographs of the as-prepared samples through the conventional hydrothermal process and proposed an APS strategy. There are not much significant differences in the surface morphologies, as Figure 1.9 clearly showed the lattice fringes with the consistent orientation of zeolite NaA morphology. However, the characteristic BET surface area and pore volume data presented in Figure 1.10 and Table 1.2 showed that the NaA zeolite synthesized from the conventional HT route has a higher surface area of 455 $m^2/g$ as compared to APS 315 $m^2/g$. The hysteresis ring in Figure 1.10a, is due to the mesoporous produced by the accumulation of zeolite. In addition, mesoporous structure is more likely to occur in atmospheric pressure system than in hydrothermal environment. The $^{29}Si$ NMR spectrum of NaA zeolite (Figure 1.10) consist of a single sharp line at nearly -89.5 ppm, in both the samples, attributed to the existence of silicon sites, which depicts the characteristics of LTA type of zeolites [35].

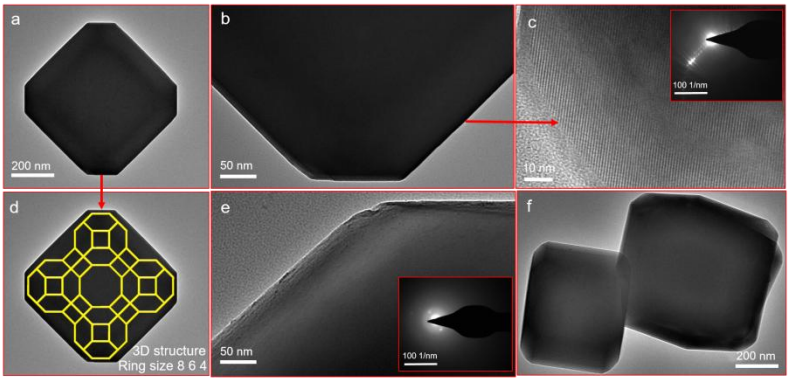


**Figure 1.9.** TEM images of NaA zeolite crystals at 120 ºC, 8 g water in gel, synthesized by an atmospheric pressure system (APS) with 0.3 g silicon oil sealant (a-d), and Hydrothermal process (e, f) with $SiO_2/Al_2O_3/Na_2O$ =1.9:1.3:1.6.

**Table 1.2.** BET physiosorption area and pore volume of zeolite CaA synthesized from ambient pressure system (APS) and hydrothermal process (HT) with $SiO_2/Al_2O_3/Na_2O$ =1.9:1.3:1.6 at 120 ºC and 8 g water in gel.

| Method | $S_{BET}(m^2/g)^a$ | $V_{total}(cm^3/g)^b$ |
|---|---|---|
| HT | 455 | 0.17 |
| APS | 315 | 0.16 |

a$S_{BET}$ (total surface area) calculated using the BET equation.

bV(total pore volume) calculated by single point method at $P/P_0$=0.95.

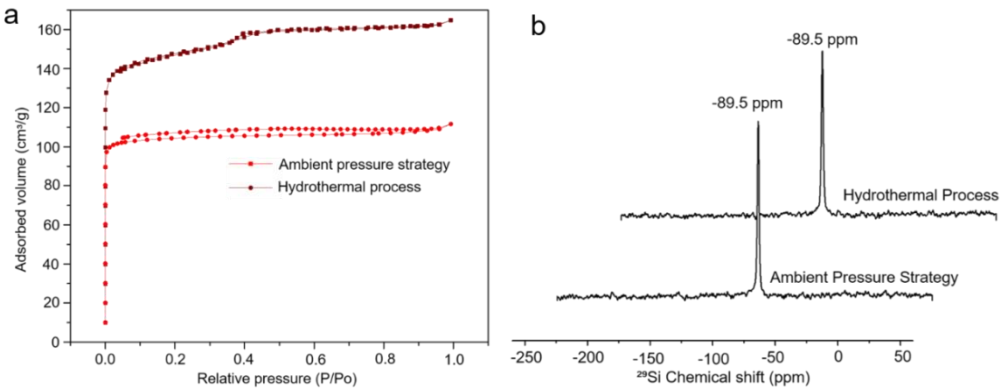


**Figure 1.10.** (a) $N_2$ physiosorption isotherm graph of CaA zeolite (b) $^{29}Si$ NMR graph of NaA zeolite synthesized by ambient pressure system (APS) with

silicon oil sealant and Hydrothermal process (HT) at 120 °C with 8 g water in gel with $SiO_2/Al_2O_3/Na_2O$=1.9:1.3:1.6.

The LTA topology is composed by combining SOD (sodalite cage) and D4R units. In the Raman spectra (Figure 1.11a), peaks around 284, 340, 412 $cm^{-1}$ corresponded to typical isotropic gel signature for all the samples. Raman bands in the range of 300-600 $cm^{-1}$ show the structure sensitivity. The prominent shift of symmetrical breathing vibration of 4 member rings at 490 $cm^{-1}$ was observed in the spectra for the samples with and without MC synthesized in HT and APS systems. Additionally, symmetrical T-O strength at 700 $cm^{-1}$ and asymmetric strength at 971, 1053, and 1104 $cm^{-1}$ clearly evidenced the formation of type A zeolite cage [36]. However, peak intensities of these samples below are slightly different which is due to the different dilutions, scattering changes, and different pressure environment effect. $^{27}Al$ spectra presented in Figure 1.11b investigated the aluminum coordination in the samples. Zeolite NaA consists of a single resonance at around 58.9 ppm which is assigned to tetrahedral Al in the framework (Figure 1.11b), which is the clear depiction of successful synthesis of LTA zeolite formation for all the samples.

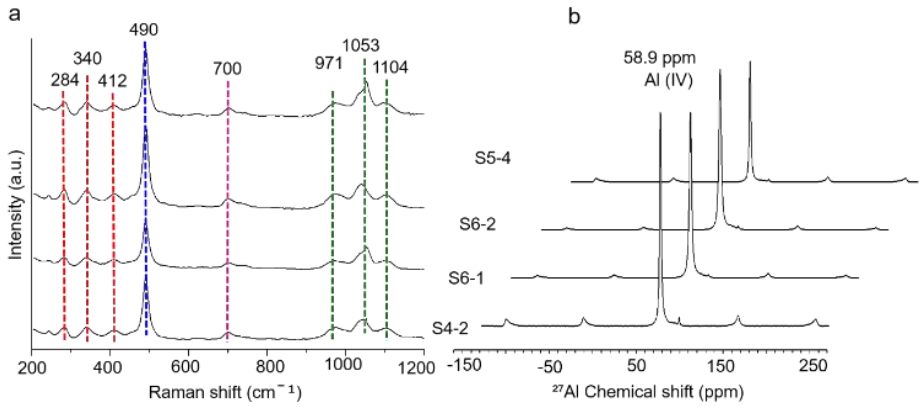


**Figure 1.11.** (a) UV-Raman spectrum (b) $^{27}Al$ NMR, for NaA synthesis for APS with MC (S5-4) and without MC template (S4-2), and hydrothermal process with no MC template (S6-1) and (S6-2) with MC, at 120 °C temperature, and 8 g water, and $SiO_2/Al_2O_3/Na_2O$=1.9:1.3:1.6.

## 1.4. Conclusions

Raising the synthesis efficacy is of high significance to lift the application of zeolites in various fields. Pure NaA zeolite has been synthesized successfully by ambient pressure synthesis (APS) method with the ratio $SiO_2/Al_2O_3/Na_2O$=1.9:1.3:1.6, optimum crystallization temperature, and period. We have provided intensive analysis on the effect of crystallization temperature, the water content in gel solution, and various sealant oil types. Highly crystalline NaA zeolite was obtained at 120 $^oC$, 8 g water content within 3 g silicon oil sealant. Moreover, methyl cellulose template has also been used to investigate its effect on crystallinity. PEG-400 sealant with 30 mg template in the APS process improved the BET surface area. A systematic comparison of APS and Hydrothermal process was also conducted for NaA zeolite synthesis and concluded with the facts that APS can produce the NaA zeolite with high efficacy and less energy as compared to the conventional hydrothermal process.

## 1.5. Associated Content

## 1.5.1 Experimental Section

### Zeolites experiment section

### Materials

$NaAlO_2$ (Sinopharm Chemical Reagent Co., Ltd.), NaOH (Shanghai Lingfeng Chemical Reagent Co., Ltd.), Tetrapropylammonium hydroxide (TPAOH, 25%, Shanghai Aladdin Bio-Chem Technology Co., Ltd), $NH_4F$ (Sinopharm Chemical Reagent Co., Ltd.), $SiO_2 \cdot xH_2O$ (17.4 wt% $H_2O$, Sinopharm Chemical Reagent Co., Ltd.), Nano-$SiO_2$ (Shanghai Aladdin Bio-Chem Technology Co., Ltd), Tetraethyl ammonium hydroxide (TEAOH, 25%, Shanghai Aladdin Bio-Chem Technology Co.,

Ltd) and H-Beta seed (Nankai catalyst Co., Ltd. China) and deionized water, All materials were used without further purification.

## Silicalite-1 (MFI) zeolite synthesis method

Added TPAOH and $SiO_2 \cdot xH_2O$ into deionized water. The mixture was stirred at 90 $^oC$ and aged for 10 h. Then, we added $NH_4F$ solution to the above solution and continued aging for another 10 h. The obtained zeolite precursor ratio is 6.4 $SiO_2$: 2.7 TPAOH: 11.9 $NH_4F$: 200 $H_2O$. Then the zeolite precursor was transferred into a tube and sealing liquid was added to the upper layer. Crystallization was carried out at 90 $^oC$ for 96 h under atmospheric pressure. The product will get after wash, dry, and calcine it.

## NaY (FAU) zeolite synthesis method

The ambient pressure method was employed for zeolite Y synthesis. In the typical synthesis of zeolite Y, two gels (seed and feedstock) were prepared. The seed gel was formulated by sequentially adding 6.48 g deionized $H_2O$, 1.51 g NaOH, and 0.50 g $NaAlO_2$ under strong stirring. 1.56 g $SiO_2 \cdot xH_2O$ was added to the mixture, stirred, and then aged for 10 min to form a uniform gel. The feedstock gel was prepared by the same procedure with 6.48 g deionized $H_2O$, 0.50 g NaOH, 0.50 g $NaAlO_2$, and 1.56 g $SiO_2 \cdot xH_2O$ to form a component gel. The seed gel was gradually added to the feedstock gel under strong stirring to obtain a complete zeolite gel. The completed gel was aged for 10 min, transferred into a glass tube, sealed with a 1.0 g liquid sealant, and later transferred into a conventional lab oven and crystallized at 90 $^oC$ for 18 h. The sample was taken out, washed with toluene and water, centrifuged, and dried at 80 $^oC$ overnight to obtain zeolite NaY.

## BEA zeolite experiment synthesis method

6 g Nano-$SiO_2$, 0.33 g $NaAlO_2$, 0.24 g NaOH, 11.8 g TEAOH and 9 g $H_2O$ were added into a beaker, then stired the gel for 3 h. Next, we added 0.3 g H-Beta seed and stired it for another 30 min. The precursor gel of the zeolite gradually pour averagely into three tubes. After added sealent, the tube was put in oven and reacted at 100 °C for 10 days, then centrifugally washed, dried, and calcined the sample at 550 °C for 5 h.

## Zeolite Characterization

X-Ray Diffraction (XRD) analysis of as-prepared samples was performed on a Rigaku Ultima IV diffractometer with Cu Kα radiation basis and data collected in 2θ = 5-50° (λ=1.54 Å, scanning rate of 5°/min at 40 kV and 40 mA). The morphologies of the synthesized zeolite were investigated with Scanning Electron Microscopy (SEM) and images of all samples were obtained on a Hitachi SU1510. The textural properties of the samples were measured by $N_2$-physisorption on an automatic gas adsorption system (Micromeritics, ASAP 2460). A mass of 0.1 g each sample was used in this process. The samples were previously degassed at 250 °C for 3 h to remove unwanted gases, organics, and water. The surface area was calculated from the Brunauer-Emmett-Teller (BET) equation whereas the pore sizes were determined by the Barrett-Joyner-Halenda (BJH) method.

## 1.5.2. Results and Characterizations

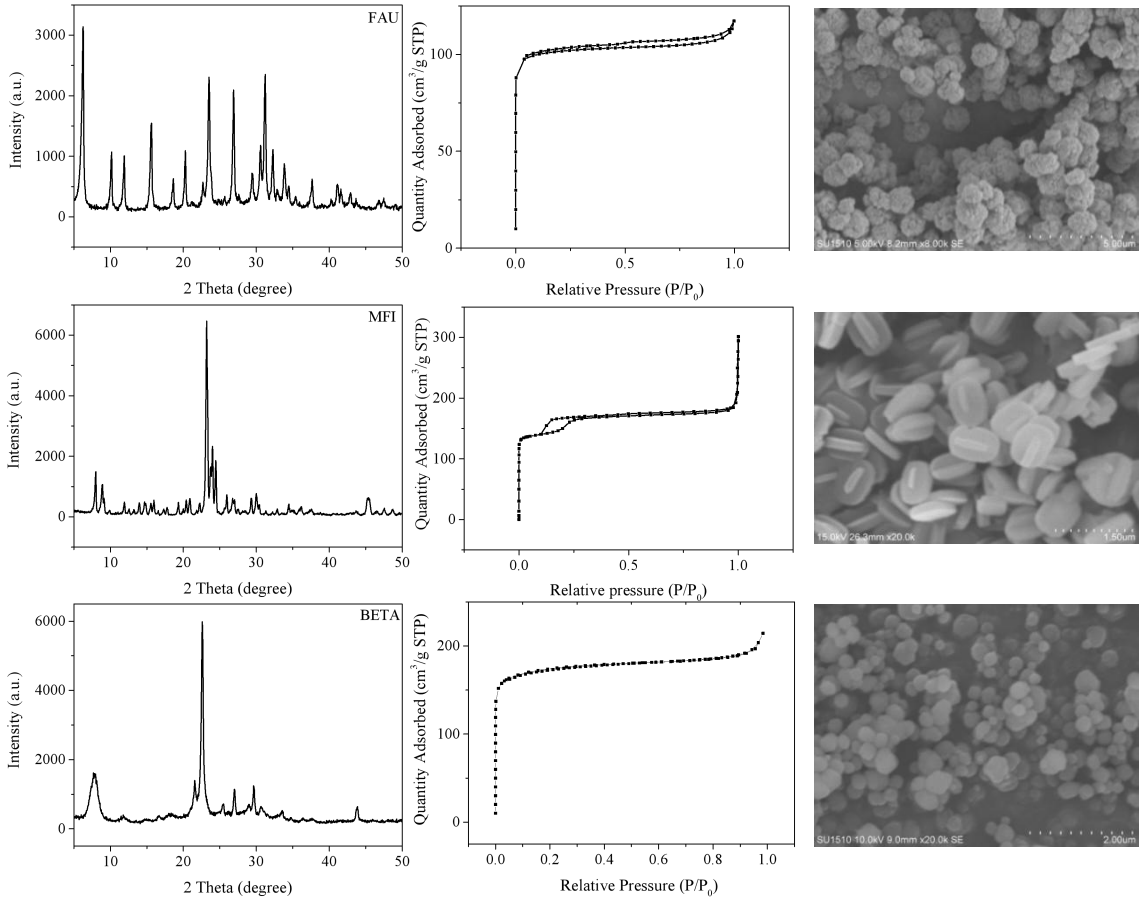


**Figure 1.12.** XRD patterns, $N_2$ adsorption & desorption patterns and SEM micrographs of FAU, MFI and BEA zeolites synthesized with APS method.

The XRD spectrum indicates that we successfully prepared FAU, MFI, and BEA zeolites via the same atmospheric pressure preparation process. The $N_2$ adsorption and desorption results indicate that FAU zeolite mainly has a microporous structure, while also containing a small amount of mesopores. However, MFI and BEA zeolites only have microporous structures. The SEM results indicate that the FAU zeolite prepared under normal pressure exhibits a spherical structure with nanosheet aggregation, with a particle size of approximately 1 μm. MFI zeolite exhibits a cross shaped structure with a thickness of approximately 200 nm. BEA zeolite has a spherical structure with a particle size of approximately 300 nm.

# References

[1] M.E. Davis, *Nature.* 417 (2002) 813-821.

[2] M. Choi, H.S. Cho, R. Srivastava, C. Venkatesan, D.-H. Choi, R. Ryoo, *Nature materials.* 5 (2006) 718-723.

[3] W.J. Roth, P. Nachtigall, R.E. Morris, P.S. Wheatley, V.R. Seymour, S.E. Ashbrook, P. Chlubná, L. Grajciar, M. Položij, A. Zukal, *Nature chemistry.* 5 (2013) 628-633.

[4] J. Han, Z. Liu, H. Li, J. Zhong, W. Zhang, J. Huang, A. Zheng, Y. Wei, Z. Liu, *ACS Catal.* 10 (2020) 8727-8735.

[5] V.J. Inglezakis, *J. Colloid Interf. Sci.* 281 (2005) 68-79.

[6] V.V. Murashov, M.A. White, *Mater Chem Phys.* 75 (2002) 178-180.

[7] M. Dusselier, M.E. Davis, *Chem. Rev.* 118 (2018) 5265-5329.

[8] C.M. Lew, R. Cai, Y. Yan, *Accounts. Chem. Res.* 43 (2010) 210-219.

[9] A. Noreen, M. Li, Y. Fu, C.C. Amoo, J. Wang, E. Maturura, C. Du, R. Yang, C. Xing, J. Sun, *ACS Catal.* 10 (2020) 14186-14194.

[10] L. Bacakova, M. Vandrovcova, I. Kopova, I. Jirka, *Biomaterials science.* 6 (2018) 974-989.

[11] M. Dakhchoune, L.F. Villalobos, R. Semino, L. Liu, M. Rezaei, P. Schouwink, C.E. Avalos, P. Baade, V. Wood, Y. Han, *Nature Materials.* 20 (2021) 362-369.

[12] K. Muraoka, Y. Sada, D. Miyazaki, W. Chaikittisilp, T. Okubo, *Nat. Commun.* 10 (2019) 4459.

[13] M. Moliner, C. Martínez, A. Corma, *Chem. Mater.* 26 (2014) 246-258.

[14] M. Severance, B. Wang, K. Ramasubramanian, L. Zhao, W.W. Ho, P.K. Dutta, *Langmuir.* 30 (2014) 6929-6937.

[15] Z. Yang, Y. Xia, R. Mokaya, *Adv. Mater.* 16 (2004) 727-732.

[16] A. Khaleque, M.M. Alam, M. Hoque, S. Mondal, J.B. Haider, B. Xu, M. Johir, A.K. Karmakar, J. Zhou, M.B. Ahmed, *Environmental Advances.* 2 (2020) 100019.

[17] H. Liu, Y. Fu, M. Li, J. Wang, A. Noreen, E. Maturura, X. Gao, R. Yang, C.C.

Amoo, C. Xing, *Journal of Materials Chemistry A.* 9 (2021) 8663-8673.

[18] J. Wang, C. Du, Q. Wei, W. Shen, *Energ. Fuel.* 35 (2021) 4358-4366.

[19] Y.C. Feng, Y. Meng, F.X. Li, Z.P. Lv, J.W. Xue, *J. Porous. Mat.* 20 (2013) 465-471.

[20] H. Chen, J. Wydra, X. Zhang, P.-S. Lee, Z. Wang, W. Fan, M. Tsapatsis, *J. Am. Chem. Soc.* 133 (2011) 12390-12393.

[21] C. Tan, Z. Liu, Y. Yonezawa, S. Sukenaga, M. Ando, H. Shibata, Y. Sasaki, T. Okubo, T. Wakihara, *Chem. Commun.* 56 (2020) 2811-2814.

[22] M. Matsukata, M. Ogura, T. Osaki, P.R. Hari Prasad Rao, M. Nomura, E. Kikuchi, *Top. Catal.* 9 (1999) 77-92.

[23] L. Ren, Q. Wu, C. Yang, L. Zhu, C. Li, P. Zhang, H. Zhang, X. Meng, F.-S. Xiao, *J. Am. Chem. Soc.* 134 (2012) 15173-15176.

[24] X. Meng, F.-S. Xiao, *Chem. Rev.* 114 (2014) 1521-1543.

[25] D. Reinoso, M. Adrover, M. Pedernera, *Ultrason. Sonochem.* 42 (2018) 303-309.

[26] P. Pal, J.K. Das, N. Das, S. Bandyopadhyay, *Ultrason. Sonochem.* 20 (2013) 314-321.

[27] L. Zhang, X. Wang, Y. Chen, *Chem. Eng. J.* 382 (2020) 122913.

[28] A. Martin-Calvo, J. Parra, C. Ania, S. Calero, *The Journal of Physical Chemistry C.* 118 (2014) 25460-25467.

[29] R.K. Parsapur, P. Selvam, *Scientific reports.* 8 (2018) 1-13.

[30] K. Cho, H.S. Cho, L.-C. de Ménorval, R. Ryoo, *Chem. Mater.* 21 (2009) 5664-5673.

[31] D. Verboekend, T.C. Keller, S. Mitchell, J. Pérez-Ramírez, *Adv. Funct. Mater.* 23 (2013) 1923-1934.

[32] Y. Ji, B. Zhang, W. Zhang, B. Zhao, H. Li, D. Wang, Y. Li, *Chem. Res. Chinese. U.* 33 (2017) 520-524.

[33] F. Collins, A. Rozhkovskaya, J.G. Outram, G.J. Millar, *Micropor. Mesopor. Mat.* 291 (2020) 109667.

[34] T.J. Cruz, M.I. Melo, S. Pergher, *Applied Sciences.* 10 (2020) 7332.

[35] H. Tounsi, S. Mseddi, S. Djemel, *Physics Procedia.* 2 (2009) 1065-1074.

[36] A. Depla, E. Verheyen, A. Veyfeyken, E. Gobechiya, T. Hartmann, R. Schaefer, J.A. Martens, C.E. Kirschhock, *Phys. Chem. Chem. Phys.* 13 (2011) 13730-13737.

# Chapter 2

# Facile synthesis of zeolites under an atmospheric reflux system

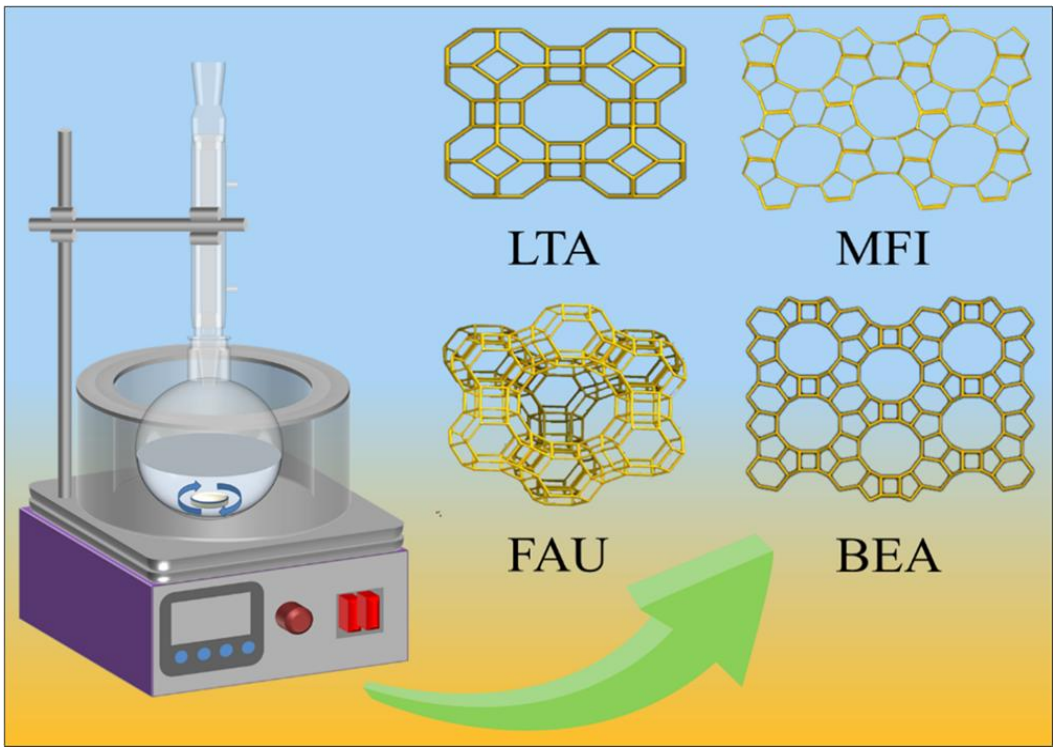


The traditional method for zeolite synthesis is challenged with high operating cost and safety issues. In the chapter 2, we detail facile synthesis of different zeolites under an atmospheric reflux system. The procedure presented in this work is green, rapid, safety and sustainable chemistry of zeolites and other porous crystalline materials.

# Abstract

Traditionally zeolites are produced under long aging processes and high autogenous pressure reactions associated with a lot of safety concerns and explosion risks. Herein, a facile zeolite synthesis method under atmospheric pressure using a reflux system is reported. The zeolite gel crystallizes rapidly under the synthesis conditions of heating, stirring, and reflux in an oil bath. We have successfully synthesized LTA, FAU, MFI, and BEA zeolites. This technique not only eliminates the potential risks associated with pressure vessels but also greatly improves the synthesis rate and speeds up the production cycle. This synthesis strategy provides a new, safe and rapid way of synthesizing zeolites.

**Keywords:** Zeolite, Facile synthesis, Reflux system, Atmospheric synthesis.

## 2.1 Introduction

Zeolites are important materials with a well-defined, crystalline structure and unique pore properties used in different fields of the chemical industry such as shape-selective catalysis, gas adsorption, and separation [1-6]. LTA as a representative zeolite has excellent ion exchange capabilities and plays a huge role in heavy metal ion exchange and waste management [7-9]. Composite polymer LTA zeolite with nanocomposite membranes may be useful in air separation too [10]. In addition, FAU, BEA and MFI zeolites are promising heterogeneous catalytic materials for the cracking and isomerization of hydrocarbons [11-13].

Due to the wide applications of zeolites, researchers began to explore the feasibility of sustainable industrial synthesis of zeolite since the 1940s. In industry, large-scale production of zeolites is usually carried out by the hydrothermal, solvothermal, solvent-free, and dry gel conversion (DGC) methods [14-17]. The solvothermal synthesis method is very similar to the hydrothermal route where the synthesis is conducted in a stainless-steel autoclave, the only difference being that the precursor solution is usually non-aqueous. However, these methods are often accompanied by longer aging times and production cycles of zeolite precursors to obtain the highly crystalline zeolites. In the production process of zeolite, a lot of energy is utilized and there is also the environmental problem of waste disposal.

The solvent-free method is a new technique in the green production of zeolites [18-20]. It's a simple procedure for synthesizing zeolites through simply mixing, grinding and crystallization of raw materials. Since no solvent is used in this method, this can effectively reduce the discharge of toxic waste liquid. However, this method is imperfect and has only stayed in the small-scale trial stage, not solving the problem of evenly mixing raw materials in scale-up production. The DGC technique has been developed as an optional procedure for zeolite synthesis and in this method, dry zeolite gel precursors are crystallized through volatile organic amines or steam. It is

difficult to achieve the industrial production of zeolites by this method because the DGC method is very inflexible on the use of solvent, any slight change in solvent use results in massive synthesis failure [5, 21, 22]. These flaws seriously hinder large-scale production of zeolite. Henceforth, there is an urgent need to explore novel synthesis procedures, which safely and effectively synthesizes zeolites in batches.

The first consideration in the zeolite synthesis method is high-pressure factor. Many pressure vessels also have been widely used to synthesize zeolite. There are huge potential safety hazards in pressure vessels during high-temperature reaction and pressure release. Accidents caused by pressure vessel explosion emerge one after another all over the world every year. Through the investigation of researchers, it is found that many zeolites can be synthesized by themselves under their own pressure, or even under ambient temperature and pressure. Therefore, we have reason to judge that pressure is not an ultimate condition for zeolite synthesis. For avoiding to pressure vessel explosion, the atmospheric pressure synthesis route is a potential new technique for zeolite synthesis. Nevertheless, there are few successful reports thus far. Amoo et al. and Wang et al separately reported a method for synthesizing NaY zeolite at low temperature and ambient pressure, but this method has two major flaws [23, 24]. It is difficult to produce in batches, and the reaction temperature is limited to less than 120 °C. In addition, silicone oil is employed as a fluid sealant during synthesis, and its application leads to secondary pollution causing waste treatment problems. Zhang et al. reported a method of preparing nano-sized Silicalite-1 by refluxing at atmospheric pressure and low temperature [25]. Although the zeolite was successfully prepared, this method used a large number of templates and nearly 30% seed to contribute to the reaction, which is difficult to be applied in industrial production. In summary, two major problems of the methods are often encountered in an ambient pressure synthesis strategy; (1) The zeolite synthesis temperature should not be too high to prevent liquid boiling and component volatilization. (2) Insufficient temperature in the synthesis system often leads to the slow nucleation rate and long

zeolite synthesis time, and even requires the addition of a large number of seeds to induce synthesis. These problems lead to difficulty in the industrial-scale synthesis of zeolites. Herein, we propose a general route for the rapid synthesis of zeolites at atmospheric pressure, in which a flask reflux device is used as a reactor, and various zeolites (LTA, FAU, BEA, MFI) are synthesized by heating, stirring, and liquid reflux.

## 2.2 Experimental Sections

### 2.2.1 Zeolites experiment section

The reflux synthesis of LTA zeolite is used as a model in this communique and the preceding results show that a large number of zeolites can be successfully synthesized by the flask reflux device at atmospheric pressure. Meanwhile, the following different reaction methods and crystallization conditions were used for comparison in the zeolite syntheses. The detailed preparation methods and characterizations of FAU, MFI and BEA are shown in the associated content.

### 2.2.2 Materials

$NaAlO_2$ (Sinopharm Chemical Reagent Co., Ltd.), NaOH (Shanghai Lingfeng Chemical Reagent Co., Ltd.), $Na_2SiO_3 \cdot 9H_2O$ (Sinopharm Chemical Reagent Co., Ltd.), $Ca(NO_3)_2 \cdot 4H_2O$ (Shanghai Lingfeng Chemical Reagent Co. Ltd.), Commercial NaA zeolite (99%, Lvxinyuan environmental protection Co., Ltd) and deionized water were used in the synthesis of NaA zeolite. All materials were used without further purification.

### 2.2.3 NaA Zeolite Synthesis Method

The following different crystallization conditions were applied respectively in the zeolite synthesis. In all these samples, the reflux system hydrothermal method was used for zeolite NaA synthesis. As a typical run of zeolite NaA synthesis, two gels

(seed liquor and feedstock liquor) were prepared. The seed liquor was prepared by sequentially adding 20 g $H_2O$, 0.029 g NaOH, and 5 g $NaAlO_2$ into a beaker under vigorous stirring. For the formation of feedstock liquor, 11 g $Na_2SiO_3 \cdot 9H_2O$ was added to a mixture containing 20 g deionized water and 0.029 g NaOH, stirred, and aged for 10 min. Under strong stirring, the seed liquor was slowly added to the feedstock liquor to obtain an overall gel of zeolite NaA. The final NaA gel was stirred continuously for 10 min, transferred into a flask with a reflux system setup. The apparatus containing the gel was put into an oil bath for crystallization under different conditions to obtain zeolite NaA. Finally, the resultant gel sample was washed with deionized water and then dried overnight to get the final form of NaA zeolite. Various composition samples in different reaction temperatures designated as NaA-X (X=50-100 representing reaction temperature) were obtained. Simultaneously, the best temperature group was selected, and the results were compared by oven atmospheric pressure reaction, hydrothermal reaction, oil bath reaction by atmospheric pressure without reflux device, and commercial NaA. It was recorded as NaA-O, NaA-H, NaA-A, NaA-C, respectively.

## 2.2.4 Relative Crystallinity Calculation

The relative crystallinity was calculated from the XRD patterns by drawing the baseline, removing the background, and fitting the peak area. Characteristic peaks were selected at 7.18°, 10.16°, 12.45°, 16.09°, 21.65°, 23.97°, 26.09°, 27.09°, 29.92°, and 34.16°. The peak areas were summed together, and the crystallinity of the zeolite with the highest total peak area was defined as 100%, making it a reference peak to compare with other zeolite peaks.

## 2.2.5 Yield Calculation of NaA zeolite

$$\text{Yield of NaA zeolite (\%)} = \frac{\text{Mass of NaA zeolite product}}{\text{Total Mass of } (Na_2O+SiO_2+Al_2O_3)} \times \text{Relative crystallinity (\%)}$$

## 2.2.6 Zeolite Characterization

X-Ray Diffraction (XRD) analysis of as-prepared samples was performed on a Rigaku Ultima IV diffractometer with Cu Kα radiation basis and data collected in 2θ = 5-50° (λ=1.54 Å, scanning rate of 5°/min at 40 kV and 40 mA). The morphologies of the synthesized zeolite were investigated with Scanning Electron Microscopy (SEM) and images of all samples were obtained on a Hitachi SU1510. The textural properties of the samples were measured by $N_2$-physisorption on an automatic gas adsorption system (Micromeritics, ASAP 2460). A mass of 0.1 g each sample was used in this process. The samples were previously degassed at 250 °C for 3 h to remove unwanted gases, organics, and water. The surface area was calculated from the Brunauer-Emmett-Teller (BET) equation whereas the pore sizes were determined by the Barrett-Joyner-Halenda (BJH) method. The existence of a large amount of $Na^+$ in NaA zeolite causes the micropores to be blocked, which affects the measurement of BET, therefore, $Na^+$ ion was transformed into $Ca^{2+}$ for improved BET measurement. 2 g of NaA zeolite was put into 70 mL, 1M $Ca(NO_3)_2$ solution and exchanged at 60 °C for 1 h, filtered, dried, and then calcined it at 400 °C for 3 h. The resultant product was CaA zeolite. UV-Raman spectra were measured with a LabRAM HR Evolution with a spectral resolution of 2 $cm^{-1}$.

## 2.3 Results and discussion

Figure 2.1a displays the reflux synthesis system device setup for zeolite synthesis. Figure 2.1b and Figure 2.1c show XRD patterns and crystallinity of NaA zeolite synthesized at different temperatures for 4 h. Notably, they exhibit characteristic peaks associated with NaA structure from 70 to 100 °C, indicating the successful synthesis of these zeolites by the reflux system route [26-28]. The sample used was named NaA-X, X being the reaction temperature. According to Figure 2.1b and Figure 2.1c, NaA-90 sample was synthesized by the reflux system route produces relatively high crystallinity. This is quite different from the synthesis temperature of

zeolitic crystals with different crystallinity. This phenomena clearly shows the direct relationship between crystallinity and synthesis temperature, and in this case, the reaction temperature of 90 °C is the most suitable for the synthesis of NaA [29-32].

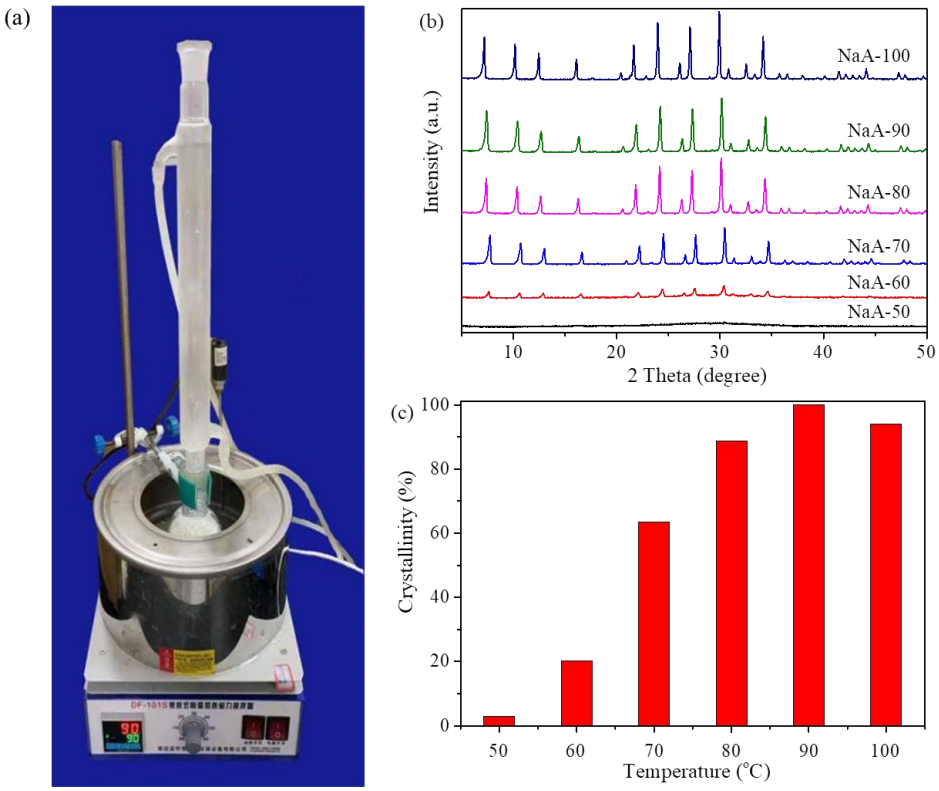


**Figure 2.1.** (a) Reflux device of NaA Zeolites synthesis, (b) XRD patterns of NaA zeolites at different reflux temperatures, (c) Crystallinity distribution of NaA zeolite at different reflux temperatures (Crystallinity of NaA-90 is noted as 100 %).

Figure 2.2a shows XRD patterns and crystallinity of NaA zeolite synthesized at 90 °C for different periods. It can be observed that the zeolite gel before heating is amorphous. With the increase in reaction time, the characteristic peaks of NaA zeolite become more noticeable indicating the gradual formation of NaA zeolite crystals with extended reaction time. The highest crystallization is observed at 4 h. Contrary, the crystallization begins to decrease at 5 h. These results indicate that 4 h of reaction gives the best crystallization results at 90 °C. Because prolonging the reaction time is easier to make the zeolite crystal sound twins and aggregate, resulting in the reduction of diffraction intensity. Figure. 2.2b shows the yield of different NaA zeolites at the

reaction time. The yield of NaA zeolite increases continuously at 0-4 h and reaches the highest at the fourth hour. At the fifth hour, the yield decreased slightly. It shows that the extension of synthesis time is not conducive to improve the yield of zeolite. Figure 2.2c shows the TEM images of NaA zeolite crystallized at 90 °C for 4 h. The cubic sections of NaA zeolite with clearly symmetrical and completely regular edges can be observed. The size of the zeolite crystal is shown to be about 1-2 μm.

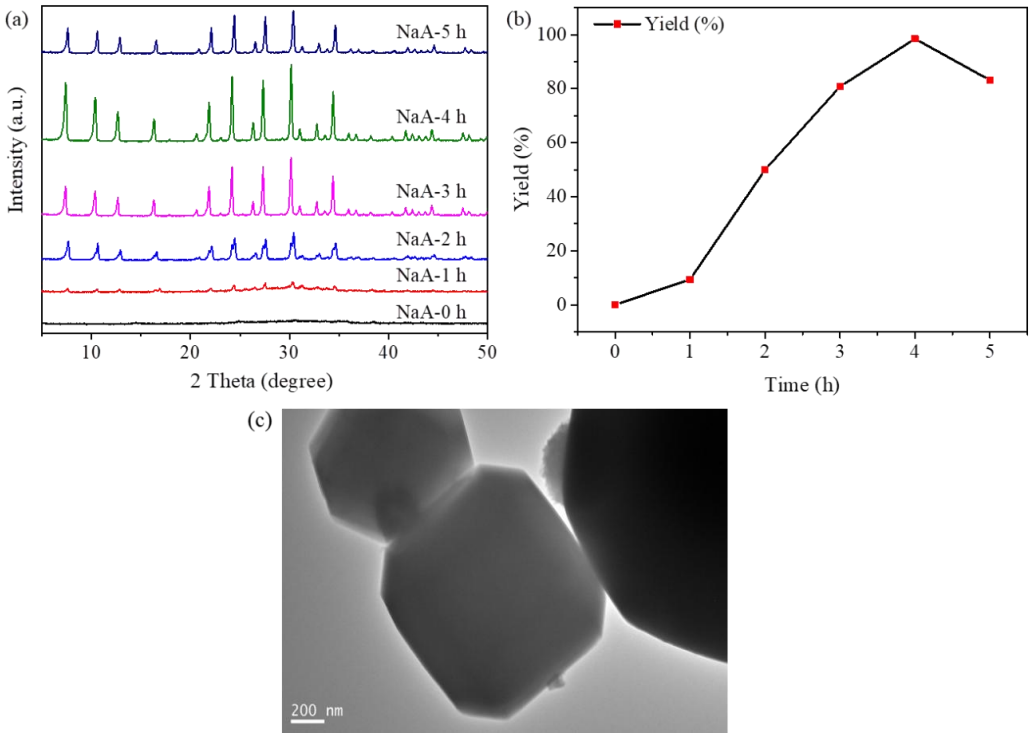


**Figure 2.2.** (a) XRD patterns of NaA zeolites for different reaction times at 90 °C, (b) Yield of NaA zeolite for different reaction times at 90 °C, (c) TEM of NaA zeolite at 90 ºC for 4 h.

Figure 2.3 shows the SEM of NaA at 90 ºC for different synthesis periods. Figure 2.3 (a)-(f) represent 0-5 h, respectively. It clearly shows that the crystallization time is the main reason affecting the crystallization behavior of zeolite. At 0-1 h, the zeolites were amorphous, and amorphous silicon and aluminum composites were clearly observed in Figure 2.3a and Figure 2.3b. At 2 h, the crystal cluster of NaA zeolite was observed in Figure 2.3c. The trace of NaA zeolite transformation, which

clearly appear on the silicon aluminum composite surface. At 3-4 h, the crystallization morphology of NaA zeolite was obvious with the extension of crystallization time, and gradually separated into a single individual. At 5 h, NaA zeolite mostly existed in the form of twins, crystal defect and aggregation. This further confirmed that the reason for the decrease of XRD diffraction peak intensity at 5 h in Figure 2.2a.

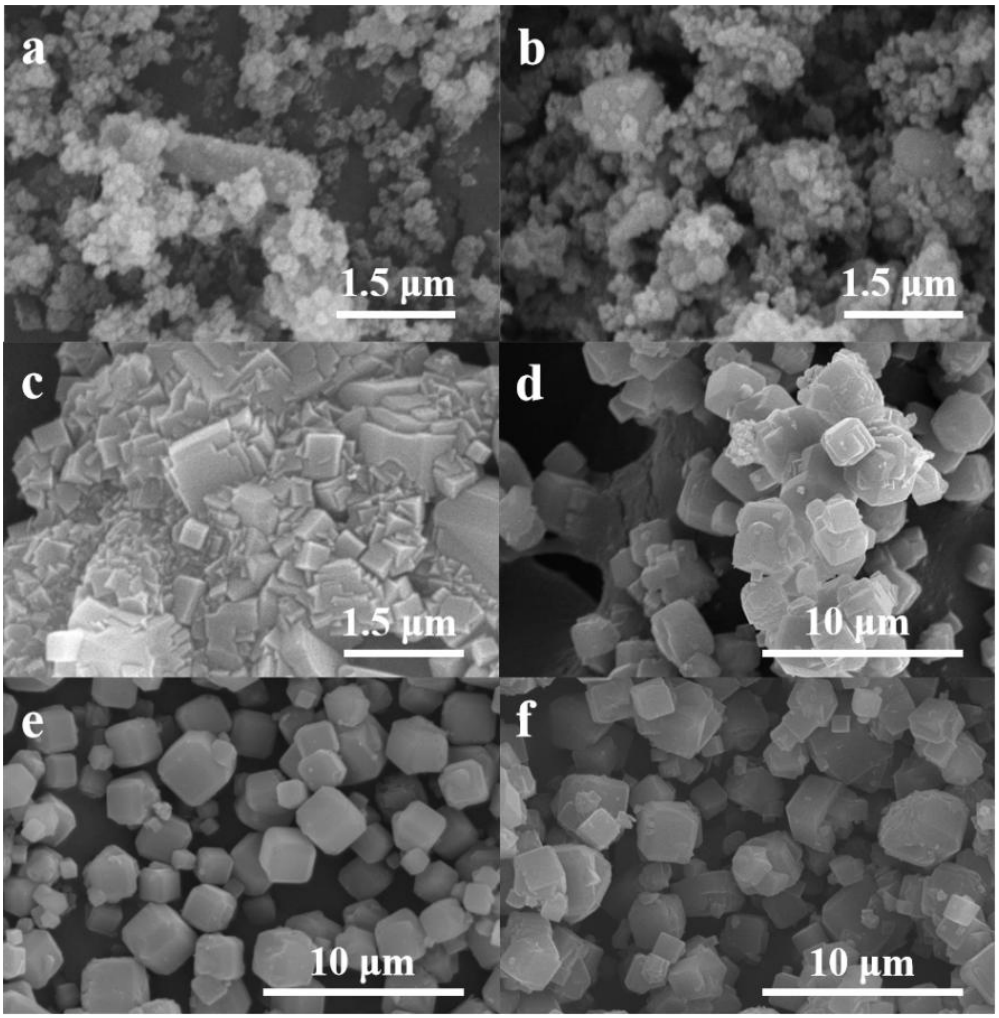


**Figure 2.3.** SEM of NaA zeolite for for different reaction times, (a) 0 h, (b) 1 h, (c) 2 h, (d) 3 h, (e) 4 h and (f) 5 h at 90 °C .

The characteristic peaks of NaA zeolite can be observed from the XRD patterns in Figure 2.4a. The results show that the NaA zeolite synthesized in the reflux system is consistent with that synthesized in other systems. According to the data in Table 2.1, among four different reaction modes, zeolites exhibit good yields in all four different

reaction modes.The crystallinity of zeolite in the reflux system (NaA-R) is the highest, even better than that of commercial NaA zeolite. The weight loss rate of the reflux reaction system is the lowest. In other words reflux system can prevent liquid loss in an unsealed state, providing a direction for the synthesis of artificial zeolites under atmospheric pressure [33]. Combined with SEM micrography, the particle size of NaA zeolite is about 1 μm [34, 35]. According to Figure 2.4b and Table 2.1, NaA zeolite is mainly microporous with a specific surface area of 317-471 $cm^2/g$. The specific surface area of NaA zeolite prepared in the reflux system is 405 $cm^2/g$, which is slightly higher than that of commercial NaA zeolite. It clarifies that the NaA zeolite prepared by the reflux system mainly has microporous structure, while commercial NaA zeolite contains a small amount of mesoporous structure [36, 37]. Figure 2.4c shows UV-Raman spectra of NaA zeolite. The peaks at 488, 340, and 278 $cm^{-1}$ are evident, indicating that NaA zeolite exhibits abundant 4 member rings (MR) and 6MR [38, 39]. There is no obvious Al-OH vibration peak at 620 $cm^{-1}$, which illustrates that Al has entered the zeolite framework [28]. Compared with other zeolites, NaA-O has the highest peak at 488 $cm^{-1}$ which clearly shows that there are more single or double quaternary ring structures on the surface of zeolite crystal monomer, so the vibration peak is strong [38, 40, 41]. Compared with commercial NaA zeolite, NaA-R zeolite shows a similar peak type, indicating complete crystallization. These observations further confirm that the reflux route is a feasible new method for the synthesis of zeolites.

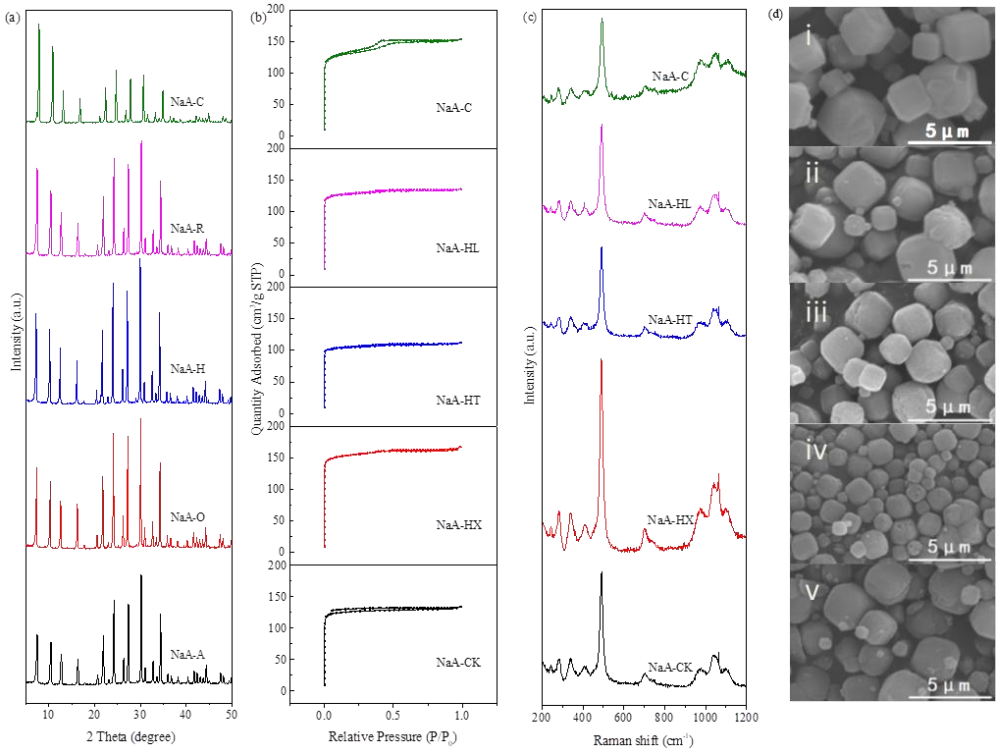


**Figure 2.4.** (a) XRD patterns, (b) $N_2$ adsorption-desorption curve, (c) UV-Raman spectra, and (d) SEM micrographs of NaA zeolite synthesized by different crystallization modes at 90 °C for 4 h. (Commercial NaA zeolite is noted by NaA-C, NaA zeolite reacted in reflux system noted by NaA-R, NaA zeolite reacted in hydrothermal method noted by NaA-H, NaA zeolite reacted in oven at ambient pressure without string noted by NaA-O, and NaA zeolite reacted in an oil bath at ambient pressure with string noted by NaA-A.)

**Table 2.1.** Pore structure, crystallinity, and mass loss of NaA zeolite.

| No. | Synthesis method | S ($m^2/g$)[a] | | | V ($cm^3/g$) | | | Crystallinity (%) | Mass loss (%) |
|---|---|---|---|---|---|---|---|---|---|
| | | Total | Micro[b] | Meso[c] | Total[d] | Micro[e] | Meso[f] | | |
| NaA-C | Commercial | 398 | 304 | 94 | 0.23 | 0.16 | 0.07 | 62.2 | 0 |
| NaA-R | Reflux | 405 | 368 | 37 | 0.22 | 0.19 | 0.03 | 100 | 1.4 |
| NaA-H | Hydrothermal | 317 | 285 | 32 | 0.17 | 0.15 | 0.02 | 92.2 | 0 |
| NaA-O | Oven | 471 | 417 | 54 | 0.25 | 0.21 | 0.04 | 87.3 | 4.3 |
| NaA-A | Ambient | 381 | 347 | 34 | 0.20 | 0.17 | 0.03 | 82.2 | 15.4 |

[a] BET surface area calculated by the BET equation.
[b] Microporous surface area evaluated by the *t*-plot method.
[c] Mesoporous surface area evaluated as $S_{Meso}=S_{Total}-S_{Micro}$.
[d] Total pore volume calculated by the single-point method at $P/P_0=0.95$ assuming complete pore saturation.
[e] Micropore volume evaluated by the *t*-plot method.
[f] Mesopore volume calculated as $V_{Meso}=V_{Total}-V_{Micro}$.

## 2.4 Conclusions

In summary, this work provides essential results on zeolites synthesis employing a reflux synthesis route. This route also enabled the successful synthesis of other types of zeolites (MFI, BEA and FAU) especially the reflux synthesis of BEA and MFI zeolite which is potentially important for shortening the synthesis time. A series of zeolites with various framework types have been successfully prepared from the reflux synthesis route through the mechanical mixing of raw materials, followed by heating in an oil bath. The products exhibit similar physical and chemical properties with the zeolites synthesized via the hydrothermal synthesis route. For industrial production of zeolites necessitated by the requirement of a huge amount of zeolites in the global market, the reflux synthesis method means a significant reduction in synthesis time, safe production, savings in energy and production costs. This methodology opens a new opportunity for synthesizing zeolites and would be potentially important for synthesizing zeolites on an industrial scale.

## 2.5. Associated Content

## 2.5.1 Experimental Section

### Zeolites experiment section

### Materials

$NaAlO_2$ (Sinopharm Chemical Reagent Co., Ltd.), NaOH (Shanghai Lingfeng Chemical Reagent Co., Ltd.), Tetrapropylammonium hydroxide (TPAOH, 25%, Shanghai Aladdin Bio-Chem Technology Co., Ltd), $SiO_2$ (Q10, Fuji Silysia Chemical Co., Ltd. Japan), $SiO_2 \cdot xH_2O$ (17.4 wt% $H_2O$), (Sinopharm Chemical Reagent Co., Ltd.), Nano-$SiO_2$ (Shanghai Aladdin Bio-Chem Technology Co., Ltd), Tetraethyl ammonium hydroxide (TEAOH, 25%, Shanghai Aladdin Bio-Chem Technology Co.,

Ltd) and H-Beta seed (Nankai catalyst Co., Ltd. China) and deionized water, All materials were used without further purification.

**Silicalite-1 (MFI) zeolite synthesis method**

10.5 g $SiO_2$, 0.5 g NaOH, and 20 g TPAOH were added into a 100 mL reflux flask. The reflux device was placed in an oil bath and stirred at the heating stage. With an increase in temperature, the precursor gel of the zeolite gradually dissolved into a liquid. The zeolite gel reacted in the reflux system at 150 ºC for 9 h, then centrifugally washed, dried, and calcined at 550 ºC for 5 h to get the final product.

**NaY zeolite (FAU) synthesis method**

In the typical synthesis of zeolite Y, two gels (seed and feedstock) were prepared. The seed gel was formulated by sequentially adding 32.4 g deionized $H_2O$, 7.55 g NaOH, and 2.50 g $NaAlO_2$ under strong stirring. 7.8 g $SiO_2 \cdot xH_2O$ was added to the mixture, stirred, and then aged for 10 min to form a uniform gel. The feedstock gel was prepared by the same procedure with 32.4 g deionized $H_2O$, 2.50 g NaOH, 2.50 g $NaAlO_2$, and 7.8 g $SiO_2 \bullet xH_2O$ to form a component gel. The seed gel was gradually added to the feedstock gel under strong stirring to obtain a complete zeolite gel. The zeolite gel was put in a 100 mL reflux bottle and heated for 4 h at 90 °C in an oil bath, then centrifugally washed, dried, and calcined it at 400 °C for 3 h to get the final product.

**Na-Beta (BEA) experiment synthesis method**

6 g Nano $SiO_2$, 0.33 g $NaAlO_2$, 0.24 g NaOH, 20 g TEAOH, and 0.75 g H-Beta seed were added into a 100 mL reflux flask. The reflux device was placed in an oil bath and stirred at the heating stage. With an increase in temperature, the precursor gel of the zeolite gradually dissolved into a liquid. The zeolite gel reacted in a reflux system at 170 °C for 24 h. After centrifugally washed and dried, we calcined it at 550 °C for 5 h to get the final product.

**Zeolite Characterization**

X-Ray Diffraction (XRD) analysis of as-prepared samples was performed on a Rigaku Ultima IV diffractometer with Cu Kα radiation basis and data collected in 2θ = 5-50° (λ=1.54 Å, scanning rate of 5°/min at 40 kV and 40 mA). The morphologies of the synthesized zeolite were investigated with Scanning Electron Microscopy (SEM) and images of all samples were obtained on a Hitachi SU1510. The textural properties of the samples were measured by $N_2$-physisorption on an automatic gas adsorption system (Micromeritics, ASAP 2460). A mass of 0.1 g each sample was used in this process. The samples were previously degassed at 250 °C for 3 h to remove unwanted gases, organics, and water. The surface area was calculated from the Brunauer-Emmett-Teller (BET) equation whereas the pore sizes were determined by the Barrett-Joyner-Halenda (BJH) method.

## 2.5.2. Results and Characterizations

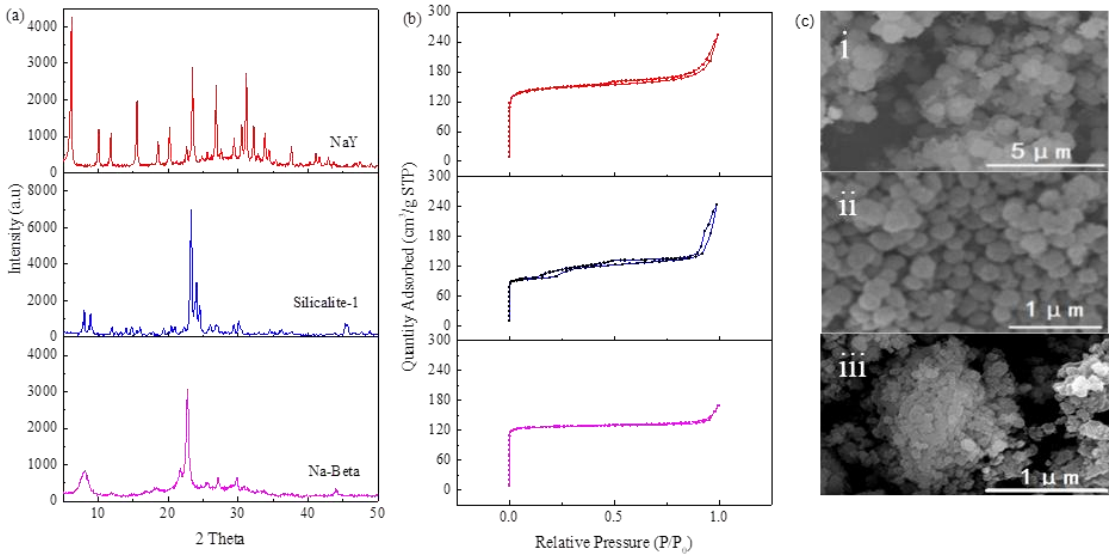


**Figure 2.5.** (a) XRD patterns, (b) $N_2$ adsorption and desorption patterns (c) SEM micrographs of NaY, Silicalite-1, and Na-Beta zeolites synthesized with a reflux system.

XRD patterns show that FAU, MFI and BEA zeolites were successfully prepared by the same reflux system process, which is faster than the APS system. The $N_2$ adsorption and desorption results indicate that FAU and MFI zeolites have a predominantly microporous structure, while also containing a small amount of mesopores. However, BEA zeolite only has a microporous structure. The SEM results indicate that the FAU zeolite prepared under atmospheric pressure exhibits a spherical structure with a particle size of approximately 1μm. MFI zeolite exhibits a spherical cross shaped structure with a particle size of approximately 300 nm. BEA zeolite exhibits a sheet-like structure.

# References

[1] F. Collins, A. Rozhkovskaya, J.G. Outram, G.J. Millar, *Micropor. Mesopor. Mat*. 291 (2020) 109667.

[2] P. Zarrintaj, G. Mahmodi, S. Manouchehri, A.H. Mashhadzadeh, M. Khodadadi, M. Servatan, M.R. Ganjali, B. Azambre, S.J. Kim, J.D. Ramsey, *MedComm*. 1 (2020) 5-34.

[3] S. Zhang, M.K. Taylor, L. Jiang, H. Ren, G. Zhu, *Chemistry–A European Journal*. 26 (2020) 3205-3221.

[4] J. Přech, P. Pizarro, D. Serrano, J. Čejka, *Chem. Soc. Rev*. 47 (2018) 8263-8306.

[5] N. Masoumifard, R. Guillet-Nicolas, F. Kleitz, *Adv. Mater*. 30 (2018) 1704439.

[6] K.O. Sulaiman, M. Sajid, K. Alhooshani, *Microchem. J*. 152 (2020) 104289.

[7] W. Li, C.Y. Chuah, S. Kwon, K. Goh, R. Wang, K. Na, T.-H. Bae, *Chemical Engineering Journal Advances*. 2 (2020) 100016.

[8] H. Shi, J. Zhang, J. Li, *RSC Adv*. 11 (2021) 5393-5398.

[9] S. Kwon, Y. Choi, B.K. Singh, K. Na, *Appl. Sur. f Sci*. 506 (2020) 145029.

[10] H. Wang, B.A. Holmberg, Y. Yan, *Journal of Materials Chemistry*. 12 (2002) 3640-3643.

[11] A. Noreen, M. Li, Y. Fu, C.C. Amoo, J. Wang, E. Maturura, C. Du, R. Yang, C. Xing, J. Sun, *ACS Catal*. 10 (2020) 14186-14194.

[12] C. Xing, M. Li, G. Zhang, A. Noreen, Y. Fu, M. Yao, C. Lu, X. Gao, R. Yang, C.C. Amoo, *Fuel*. 285 (2021) 119233.

[13] H. Liu, Y. Fu, M. Li, J. Wang, A. Noreen, E. Maturura, X. Gao, R. Yang, C.C. Amoo, C. Xing, *Journal of Materials Chemistry A*. 9 (2021) 8663-8673.

[14] Y. Wang, H. Duan, Z. Tan, X. Meng, F.-S. Xiao, *Dalton T*. (2020).

[15] C.S. Cundy, P.A. Cox, *Chem. Rev*. 103 (2003) 663-702.

[16] X. Meng, F.-S. Xiao, *Chem. Rev*. 114 (2014) 1521-1543.

[17] M. Gharibeh, G.A. Tompsett, K.S. Yngvesson, W.C. Conner, *The Journal of Physical Chemistry B*. 113 (2009) 8930-8940.

[18] Y. Ma, S. Han, Q. Wu, L. Zhu, H. Luan, X. Meng, F.-S. Xiao, *Catal. Today*. (2020).

[19] Y. Wang, H. Duan, Z. Tan, X. Meng, F.-S. Xiao, *Dalton T.* 49 (2020) 6939-6944.

[20] W. Luo, X. Yang, Z. Wang, W. Huang, J. Chen, W. Jiang, L. Wang, X. Cheng, Y. Deng, D. Zhao, *Micropor. Mesopor. Mat*. 243 (2017) 112-118.

[21] J. Čejka, R. Millini, M. Opanasenko, D.P. Serrano, W.J. Roth, *Catal. Today*. 345 (2020) 2-13.

[22] A. Kornas, J.E. Olszówka, P. Klein, V. Pashkova, *Catalysts.* 11 (2021) 246.

[23] C.C. Amoo, M. Li, A. Noreen, Y. Fu, E. Maturura, C. Du, R. Yang, X. Gao, C. Xing, N. Tsubaki, *ACS Applied Nano Materials*. 3 (2020) 8096-8103.

[24] J. Wang, M. Li, Y. Fu, C.C. Amoo, Y. Jiang, R. Yang, X. Sun, C. Xing, E. Maturura, *Micropor. Mesopor. Mat*. (2021) 111073.

[25] L. Zhang, X. Wang, Y. Chen, *Chem. Eng. J*. 382 (2020) 122913.

[26] X.-d. Liu, Y.-p. Wang, X.-m. Cui, Y. He, J. Mao, *Powder Technol*. 243 (2013) 184-193.

[27] X. Zhang, D. Tang, G. Jiang, *Adv. Powder Technol.*24 (2013) 689-696.

[28] Y. Xiao, N. Sheng, Y. Chu, Y. Wang, Q. Wu, X. Liu, F. Deng, X. Meng, Z. Feng, *Micropor. Mesopor. Mat*. 237 (2017) 201-209.

[29] M. Mirfendereski, T. Mohammadi, *Proceedings of the World Congress on Recent Advances in Nanotechnology*. (RAN'16) 2016, pp. 1-8.

[30] P. Sharma, J.-g. Yeo, M.H. Han, C.H. Cho, *RSC Adv*. 2 (2012) 7809-7823.

[31] A.Á.B. Maia, R.F. Neves, R.S. Angélica, H. Pöllmann, Synthesis, *Appl. Clay. Sci.* 108 (2015) 55-60.

[32] Y. Li, T. Peng, W. Man, L. Ju, F. Zheng, M. Zhang, M. Guo, *RSC Adv*. 6 (2016) 8358-8366.

[33] B. Bayati, A. Babaluo, R. Karimi, *J. Eur. Ceram. Soc*. 28 (2008) 2653-2657.

[34] A. Shoumkova, V. Stoyanova, *J. Porous. Mat*. 20 (2013) 249-255.

[35] Z. Yang, Y. Liu, C. Yu, X. Gu, N. Xu, *J. Membrane. Sci*. 392 (2012) 18-28.

[36] K. Menad, A. Feddag, K. Rubenis, *RASAYAN. J. Chem*. 9 (2016) 788-798.

[37] Y.C. Feng, Y. Meng, F.X. Li, Z.P. Lv, J.W. Xue, *J. Porous. Mat*. 20 (2013) 465-471.

[38] L. Ren, C. Li, F. Fan, Q. Guo, D. Liang, Z. Feng, C. Li, S. Li, F.S. Xiao, *Chemistry–A European Journal*. 17 (2011) 6162-6169.

[39] A. Depla, E. Verheyen, A. Veyfeyken, E. Gobechiya, T. Hartmann, R. Schaefer, J.A. Martens, C.E. Kirschhock, *Phys. Chem. Chem. Phys*. 13 (2011) 13730-13737.

[40] Y. Yu, G. Xiong, C. Li, F.-S. Xiao, *Micropor. Mesopor. Mat*. 46 (2001) 23-34.

[41] X. Liu, *Infrared and Raman spectroscopy.* Springer2009, pp. 197-222.

# Chapter 3

# Ultrafast Green Synthesis of Sub-micron Silicalite-1 Zeolites by a Grinding Method

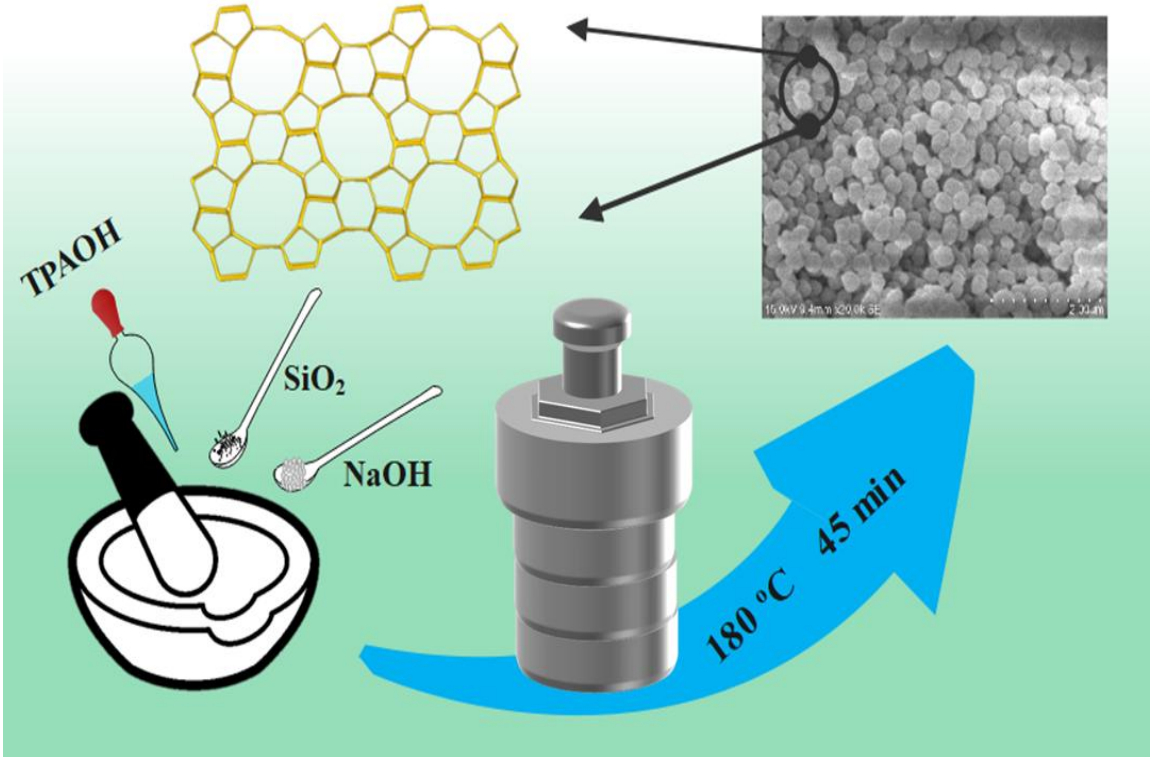


The traditional methods for synthesizing highly crystalline siliceous zeolite are challenged with high operating cost, lengthy synthesis time, and environmental issues. In the chapter 3, we detail a facile novel procedure to synthesize sub-micron Silicalite-1 zeolite with improved pore properties. The procedure presented in this work is reliable, environmentally friendly, and cost-effective when compared with the traditional synthesis method.

# Abstract

Sub-micron Silicalite-1 zeolite is traditionally synthesized by a prolonged synthesis approach which takes several days to complete. We herein demonstrate a rapid solvent-free synthesis route for sub-micron Silicalite-1 zeolite using TPAOH as an organic template to control the triple stage crystal growth rate and crystal morphologies of Silicalite-1 without the assistance of crystal seeds. This procedure is only achieved through simple mixing and grinding of raw materials and crystallization at 180 °C for 45 min. The fast synthesized Silicalite-1 zeolite proved to have higher crystal phases compared with the conventionally synthesized product. Through the absence of using additional solvents, all reactants were ultimately utilized without any waste, resulting in not only effectively reducing the cost of siliceous zeolites synthesis but also minimizing its environmental impact.

**Keywords:** Silicalite-1 zeolite, Sub-micron, Solvent-free, Ultrafast synthesis.

# 3.1 Introduction

Zeolites are microporous, crystalline aluminosilicate framework materials composed of tetrahedral metal oxide units ($AlO_4^{5-}$) and ($SiO_4^{4-}$) linked via oxygen atoms, which form a three-dimensional network containing well-defined pores and cavities of molecular dimensions [1-5]. Zeolites are useful inorganic materials that have been widely used for C1 chemistry catalysis, gas separation, ion exchange, and adsorption processes because of their versatile aligned pore structure, large specific surface area, strong hydrothermal stability, adjustable acid sites, and exchangeable positive ion [6, 7]. Most zeolites are synthesized under hydrothermal process from conventional amorphous aluminosilicate gels. Recently, hydrophobic zeolites without aluminium content have attracted much more attention on their excellent performance in catalytic reactions such as the conversion of methanol to olefins (MTO) and the selective catalytic reduction (SCR) of $NO_x$ as well as playing an important role as adsorbents because of their uniform pore structure, high specific surface area, and high thermal stability [8-10]. The silica content and synthesis procedure affect the overall features of the zeolite crystal and its functions [11, 12]. An aluminium-free zeolite, which has an extremely simple chemical composition of silica ($SiO_2$), high thermal and chemical stability, and unique shape selectivity is known as Silicalite-1 [13].

During the past decade, research on Silicalite-1 has mainly focused on its crystallization mechanism in addition to adjustable crystal morphology and to a lower extend particle size, which exerts a sizable control on the properties and performance of zeolites. The crystallization processes of zeolites can also be hastened by hydroxyl free radicals under hydrothermal conditions [14, 15].

Silicalite-1 is a hydrophobic, high silica MFI structure type zeolite, considered a promising membrane material in addition to industrial applications in areas of sensors and bio-medicine [16-18]. Silicalite-1 is often used as a model system in studies attempting to elucidate aspects of the mechanism of hydrothermal crystal growth [19].

Some researchers have devoted themselves to synthesizing highly crystalline Silicalite-1 zeolite without the use of organic templates or utilizing inexpensive raw materials, however, the final product's crystal size is usually over 5 μm [20, 21]. Furthermore, to obtain highly crystalline Silicalite-1, generally, 24-48 h should be employed at 180 $^{o}$C [13, 22]. Solvents, crystal seeds, and organic templates are widely utilized in zeolite synthesis to stimulate the dispersion and reaction of the zeolitic cell [23]. Generally, the synthesis of zeolites with the aid of crystal seeds requires an organic template and a long pretreatment time at low temperatures [24]. Synthesis of Silicalite-1 requires at least a source of silica and a template of tetrapropyl ammonium (TPA) salts. For instance, quaternary ammonium salts, like TPABr (tetrapropylammonium bromide) or TPAOH (tetrapropylammonium hydroxide), are normally employed to promote the nucleation and crystallization of Silicalite-1 [25-27]. Therefore, the organic template as a structure-directing agent is essential in the synthesis of Silicalite-1. However, reducing the amount of organic template used in the synthesis of Silicalite-1 is essential in lowering the production cost and minimizing environmental pollution [28].

Silica is the building block for the preparation of Silicalite-1 and is soluble in alkali (NaOH) [29, 30]. The greatest advantage of using NaOH for the preparation of zeolites is that high alkalinity promotes nucleation and reduces particle size, in addition to its low cost [31]. However, the major disadvantage of the NaOH method is that high alkalinity often reduces yield [32]. Furthermore, the effluent generated from the NaOH method has to be neutralized with acid to lessen undesirable environmental impact. Yang et al. reported a green synthesis method of S1 zeolite from recycled mother liquor [13]. With the increase of alkali concentration, the particle size of Silicalite-1 zeolite decreases. Although the mother liquor circulation method improves the utilization of the template, a large number of high concentration sodium hydroxide solution (6M NaOH) is used in the preparation of silica source and zeolite synthesis. Using the solvothermal method, each process inevitably produces high concentration alkaline wastewater. In addition, the whole preparation process is complex and

requires a long time on aging and crystallization cycle, hence not suitable for industrial production.

Simple techniques for Silicalite-1 zeolite preparation are employed for the practical production of the zeolite. Compared with the traditional synthesis procedures, the solvent-free synthesis of zeolites is typically sustainable, exhibiting vivid advantages as follows: (i) High yields. Silicates and aluminates has dissolved in the zeolite mother solution during conventional hydrothermal synthesis, therefore solvent-free synthesis greatly reduces these losses [33]. It leads to the yield of the zeolite using a solvent-free method is about 90−95% (based on $SiO_2$), which is much higher than that of the traditional hydrothermal method (80−86%) [34, 35]. (ii) Better utilization of reactor space. Most of the space in reactors has been generally occupied by a large amount of water in the hydrothermal synthesis. On the contrary, this does not need to be considered in solvent-free synthesis routes. Wu et al. reported the weight of the beta product is almost 14 times via solvent-free route that of a conventional hydrothermal synthesis in the same autoclave [36]. (iii) A remarkable reduction of pollutants. Avoidance of water addition in the synthesis sharply reduces the formation of liquid wastes [37]. (iv) Improved security. The lack of solvent in the zeolite crystallization effectively decreases the pressure in reactors, reducing the risk of reactor explosion. (v) The solvent-free route reduces aging time and simplifies the preparation process of zeolite due to the absence of a solvent. In 2012, a novel and generalized solvent-free route was reported by Fengshou Xiao group for synthesizing silica and aluminosilicate zeolites by the simply physical grinding of solid raw materials, followed by heating and crystallize, where it is not necessary to add any solvent [38]. The solvent-free method was later widely used to prepare aluminum phosphate-based zeolites [39].

Sub-micron material is a new concept in the materials industry, which is a highly attractive area of scientific research, playing an increasingly important role in various fields [40]. Sub-micron LTA and FAU zeolites have a large diffusion coefficient, higher diffusion capacity, and ion exchange capacity due to small particle size and

diffusion path section. Among them, sub-micron FAU zeolites also show excellent hydrogen transfer performance in fluid catalytic cracking (FCC) reactions [41-44]. Sub-micron SAPO-34 and SSZ-13 zeolites have small acid sites, which reduce carbon deposition reactions and improve the catalytic lifetime of the zeolites [45, 46]. The sub-micron ZSM-5 zeolite shortens the crystallization time due to the smaller particle size and improves the selectivity of toluene and xylene in the toluene imbalance reaction due to more exposure to acidic sites [47]. Zhang et al. successfully synthesized sub-micron ZSM-5 zeolites in 2 h by using homemade nano spherical silica and dry gel conversion method. The prepared zeolite was then applied in an aqueous phase eugenol hydrodeoxygenation reaction [48]. Sub-micron-sized Silicalite-1 crystals with uniform size are regarded as ideal models for deep study on size-dependent zeolite catalysts. However, there are few successful reports on the fastest synthesis route of sub-micron Silicalite-1, henceforth, the efficient and green synthesis is a field worth further studying it.

In this work, we will focus on describing the rapid synthesis route of sub-micron Silicalite-1 zeolite by a green solvent-free procedure. With the aid of TPAOH combined as an organic template, the solvent-free synthesis route maximizes the sustainable advantages highlighted above and the effect of the amount of template on the crystallization of Silicalite-1 has also been investigated in detail. Furthermore, we observed that the rapid solvent-free synthesis procedure shows novel insights into the crystallization process of zeolites. In addition to these features, the solvent-free method can also be combined with other sustainable strategies for synthesizing zeolites [49, 50]. The solvent-free synthesis of Silicalite-1 zeolite structure was generated by mechanically mixing solid raw materials with the effect of adding the TPAOH template investigated in detail.

## 3.2 Experimental Section

The Silicalite-1 zeolite can be successfully synthesized via a solvent-free method, which used as a model in this communique and the preceding results introducted in

detail. The detailed preparation methods and characterizations of Silicalite-2 and ZSM-22 are shown in the associated content.

## 3.2.1 Materials

$SiO_2$ (Q10, Fuji Silysia Chemical Ltd. Japan), tetrapropylammonium hydroxide (TPAOH, 25%wt, Shanghai Aladdin Bio-Chem Technology Co., Ltd), and NaOH, (Sinopharm Chemical Reagent Co., Ltd. China). All materials were used without further purification.

## 3.2.2 Silicalite-1 Synthesis

During the solvent-free synthesis of Silicalite-1, milled 2.1 g $SiO_2$, 0.1 g NaOH, and 0.5-4.0 g TPAOH solution were added into an agitator mortar respectively, and mechanically ground for 5 min at room temperature to obtain a uniform powder, with a molar ratio of $7.0SiO_2$:0.50NaOH:(0.12-0.98)TPAOH:(4.17-33.33)$H_2O$. Then the powder was transferred to a 10 mL Teflon stainlesssteel autoclave and crystallized at 180 °C for varied periods (0.5 h-48 h). The autoclave was cooled to room temperature. The product was washed and filtered, followed by drying at 80 °C and calcined at 550 °C for 5 h to obtain the sub-micron Silicalite-1 zeolite.

## 3.2.3 Characterization

X-Ray Diffractions (XRD) of as-prepared samples were performed on a Rigaku Ultima IV diffractometer with Cu Kα radiation basis and data collected in $2\theta$ = 5-50° ($\lambda$=1.54 Å, scanning rate of 5°/min at 40 kV and 40 mA). The morphologies of the synthesized zeolite were investigated with Scanning Electron Microscopy (SEM) and images of all samples were obtained on a Hitachi SU1510. The textural properties of the samples were measured by $N_2$-physisorption on a Micromeritics ASAP 2460. A mass of 0.1 g of each sample was used in this process. The samples were previously degassed at 250 °C for 3 h to remove unwanted gases, organics, and water. The

surface area was calculated from the Brunauer-Emmett-Teller (BET) equation. UV-Raman spectra were measured on a Horiba LabRAM HR Evolution fully achromatic spectrometer with a spectral resolution of 2 $cm^{-1}$.

## 3.3 Results and Discussion

The XRD patterns and SEM images of zeolite samples crystallized at 180 °C at different times of 4 to 48 h are shown in Figure 3.1. The corresponding XRD patterns in Figure 3.1a show strong characteristic peaks of MFI type zeolite at different times of crystallization from 4 to 48 h. The SEM images of the prepared Silicalite-1 zeolite displayed in Figure 3.1b clearly show an MFI crystal phase. From 4 to 48 h, Silicalite-1 zeolite has completed crystallization and obtained good crystallinity. It can be observed on SEM micrographs that the particle size of Silicalite-1 does not change significantly with the extension of crystallization time. This also shows that under this synthesis method, the synthesis time of Silicalite-1 can be further shortened.

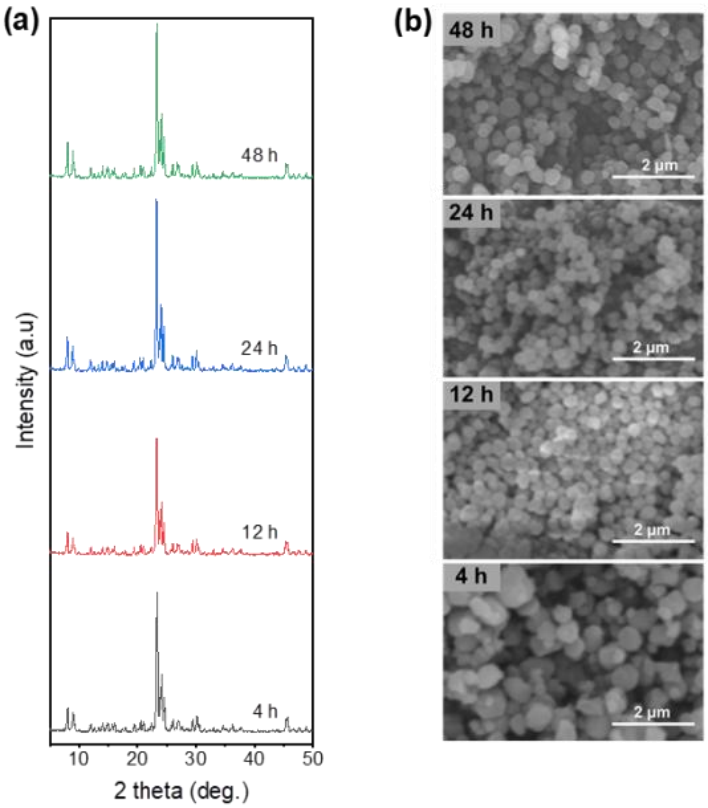


**Figure. 3.1.** (a) XRD patterns, (b) SEM images of as-prepared Silicalite-1 zeolite

samples crystallized at different periods at 180 °C， 7 $SiO_2$: 0.5 NaOH: 0.98 TPAOH: 33.3 $H_2O$.

The XRD patterns presented in Figure 3.2 indicate that the crystallization of Silicalite-1 zeolite is temperature-dependent. The diffractograms show that when crystallization is performed at 100 °C and 120 °C, only amorphous zeolite phases are observed. However, when the crystallization temperature is extended to 140 °C, the MFI characteristic peaks appear at 4 h. When the crystallization temperature is extended to 160 °C, Silicalite-1 zeolite begins to crystallize within 45 min and is successfully synthesized in 1 h. At 180 °C complete Silicalite-1 peaks are observed earlier than those at 140 °C and 160 °C, beginning to show the highest intensity at 45 min. When the crystallization temperature is further extended to 200 °C, the intensity of Silicalite-1 characteristic peak initially increases and then gradually decreases with prolonged crystallization periods. There is a further increase in energy consumption and equipment use at higher crystallization temperatures. Therefore, these results show that synthesizing at 180 °C for 45 min is the best and economic synthesis condition for sub-micron Silicalite-1 zeolite.

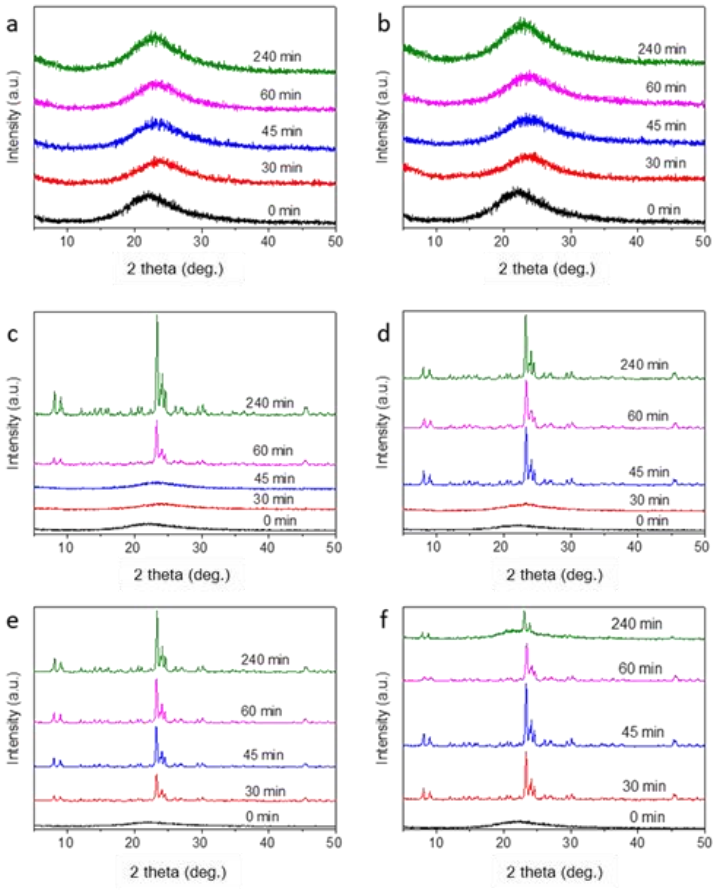


**Figure 3.2.** XRD patterns of as-prepared Silicalite-1 zeolite samples with 4 g TPAOH solution prepared at different crystallization temperatures for different periods. (a) 100 °C, (b) 120 °C, (c) 140 °C, (d) 160 °C, (e) 180 °C, (f) 200 °C, 7 $SiO_2$: 0.5 NaOH: 0.98 TPAOH: 33.3$H_2O$.

Figure 3.3 shows XRD diffractograms and SEM micrographs of various amounts of the template on Silicalite-1 with particle size distribution crystallized at 45 min. The peak distribution still follows an MFI structured zeolite pattern. Weak MFI characteristic peaks are observed when small template amounts are employed (0.0-1.0 g). Sharp peaks depicting MFI zeolite patterns are observed when 1.5 g to 4.0 g of TPAOH is used although there is not much significant difference in the crystal peaks observed when 1.5 g, 2.0 g, and 4.0 g TPAOH is added. SEM images further prove that the main factor regulating the crystal size of Silicalite-1 zeolite is the amount of organic template used.

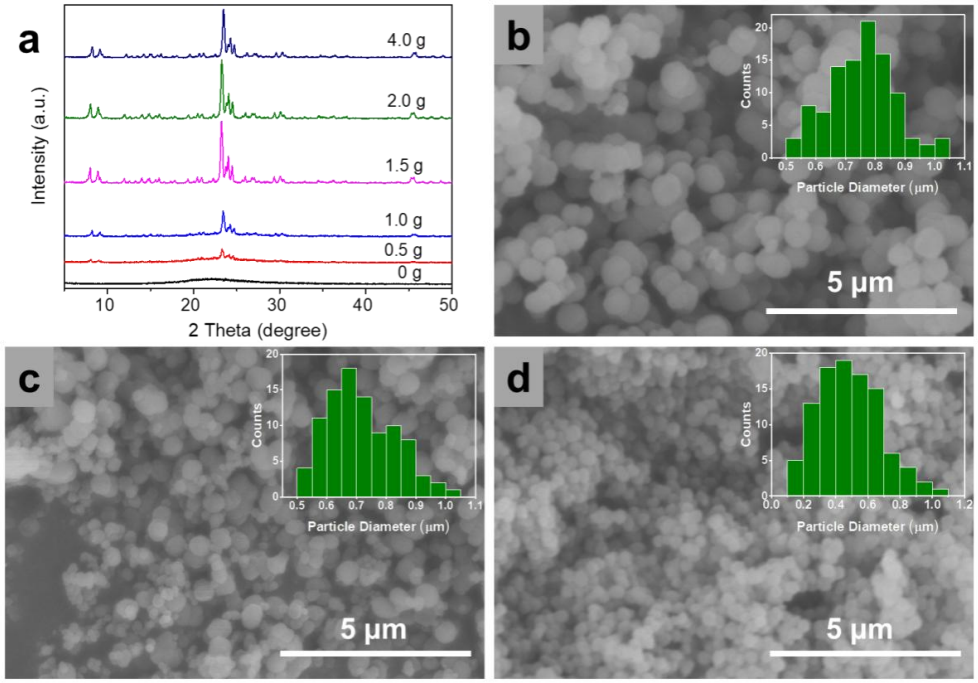


**Figure 3.3.** (a) XRD patterns of as-prepared Silicalite-1 zeolite samples with different mass TPAOH solution prepared at 180 °C for 45 min. (b-d) SEM images of as-prepared Silicalite-1 treated with different TPAOH amounts, (b) 1.5 g, (c) 2.0 g, (d) 4.0 g, crystallized for 45 min.

Figure 3.4 and Table 3.1 show the $N_2$ adsorption-desorption curve, pore size distribution, and yield of Silicalite-1 zeolite. The zeolite prepared by the grinding method has predominantly microporous and mesoporous structures. With an increase in the mass of template, the specific surface area and pore volume of zeolite increases. The mesoporous structure and yield of zeolite also decreases gradually. The reason for the decrease in yield of zeolite is that, with an increase in the amount of template, the grinding state changes from dry powder to wet powder, and some precursors are attached to the inner wall of the mortar, resulting in a small amount of loss. However, the yield of Silicalite-1 zeolite remained above 85%. The low-pressure hysteresis loop at $P/P_0$=0.2 is a unique phenomenon of MFI zeolite [51, 52]. This often appears in pure silicon or high silicon MFI zeolite, which is due to the formation of monoclinic systems at the same time in the crystallization process of zeolites. The stepped shape and low-pressure hysteresis ring appear in the adsorption isotherm.

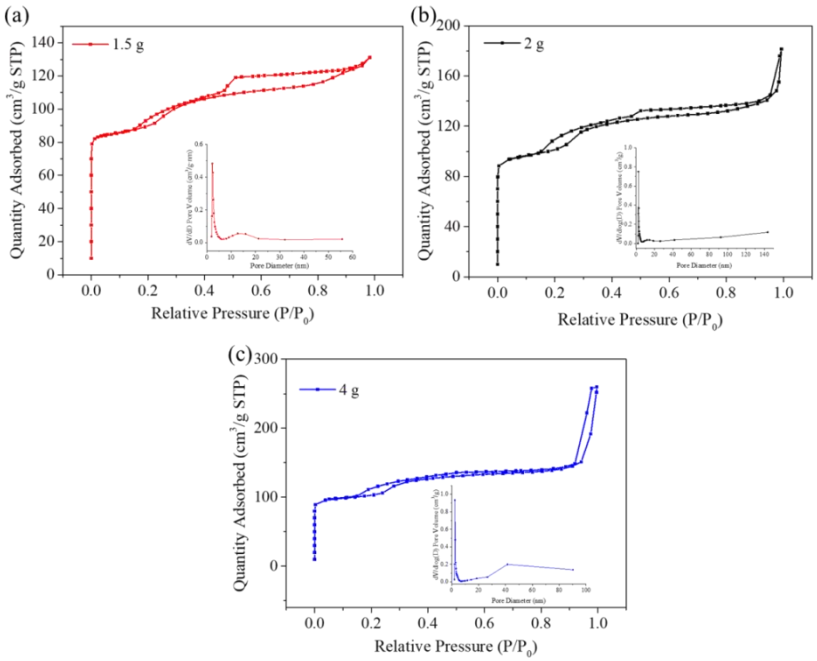


**Figure 3.4.** $N_2$ adsorption-desorption curve and pore size distribution of Silicalite-1 zeolites with different template mass. (a) 1.5 g, (b) 2.0 g, (c) 4.0 g, crystallized for 45 min.

**Table 3.1.** Pore structure and yield of Silicalite-1 zeolites with different template mass.

| Template mass/g | $S_{BET}$($m^2g^{-1}$) | | | V ($cm^3g^{-1}$) | Yield (%) |
|---|---|---|---|---|---|
| | $S_{Total}$ | $S_{Micro}$ | $S_{External}$ | Total | |
| 1.5 | 300 | 207 | 93 | 0.19 | 91 |
| 2 | 351 | 230 | 121 | 0.21 | 90 |
| 4 | 374 | 248 | 125 | 0.24 | 85 |

Figure 3.5 displays the effect of different grinding time on the crystallization of Silicalite-1 zeolite. The XRD patterns display that the crystallinity of Silicalite-1 zeolite gradually decreases with the extension of grinding time. When the grinding time is 30 min, the amorphous product is obtained. Therefore, 5 min is the best preparation time.

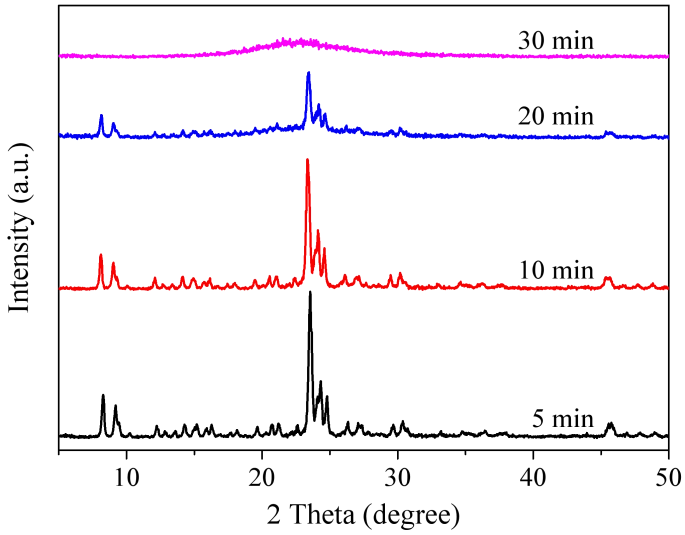


**Figure 3.5.** Effects of grinding time on the crystallization of Silicalite-1 zeolite at 180 °C for 45 min, 7 $SiO_2$: 0.5 NaOH: 0.37 TPAOH: 12.5$H_2O$.

Figure 3.6a shows XRD diffractograms demonstrating the subsequent transformation of the silicate gel as the crystallization time increases from 30 to 240 min. Notably, the patterns exhibit characteristic peaks associated with an MFI structure from 45-240 min, indicating the successful synthesis of sub-micron Silicalite-1 zeolite from the solvent-free route at this time interval. This observation is directly related to the transformation of the solid phase of reactants during the synthesis where the solids or particles aggregate with each other forming notable polycrystals.

Figure 3.6b shows the BET of Silicalite-1 at different synthesis periods. Before 40 min, only mesopores exists in the $N_2$ adsorption-desorption curve. At 40 min, the $N_2$ adsorption-desorption curve shows a noticeable micropore structure, indicating the beginning of crystallization. After 45 min, the $N_2$ adsorption-desorption curves tend to be stable, with similar microporous and mesoporous structures.

Figure 3.6c shows UV-Raman spectra of Silicalite-1 at different reaction periods. The solid phase of the synthesis framework of sub-micron Silicalite-1 indicates that synthesis species are incorporated into silicate species, and the polymeric silicate

species are depolymerized into monomeric silicate species during the early stage of zeolite formation. After reaction at 180 °C for 30 min, there are no noticeable changes in UV-Raman bands which is in accordance with the high disordering of 4 member rings (MR) with strong Raman signals by the high dispersion of solid salts on the amorphous support [53]. After crystallization for 40 min during the transformation to MFI, the Raman bands associated with the characteristic vibrations of the MFI zeolite framework (433 and 475 $cm^{-1}$ for 4MR, 289 $cm^{-1}$ for single 6MR, and 377 $cm^{-1}$ for the 5MR units in the crystal phase) gradually appear [54, 55]. With the crystallization time increasing, the intensities of XRD peaks and Raman bands strongly increase, indicating the successful transformation from amorphous silica to zeolite crystals. Correspondingly, the degree of silica condensation for the samples is extensively enhanced. When the crystallization time is over, there are no noticeable changes in XRD patterns and UV-Raman spectra of the samples, indicating that the crystallization of Silicalite-1 zeolite is complete. At 45 min, the UV-Raman spectra tend to be stable and consistent with the peak height at 60 min. When the crystallization time is 240 min, the intensity of the characteristic peak decreases, and the internal structure of Silicalite-1 zeolite begins to decompose and recombine, which indicates that a long crystallization time is not preferably suitable for the synthesis of Silicalite-1 zeolite. These results demonstrate that Silicalite-1 zeolite crystallized through the solid phase transformation was successfully synthesized in 45 minutes.

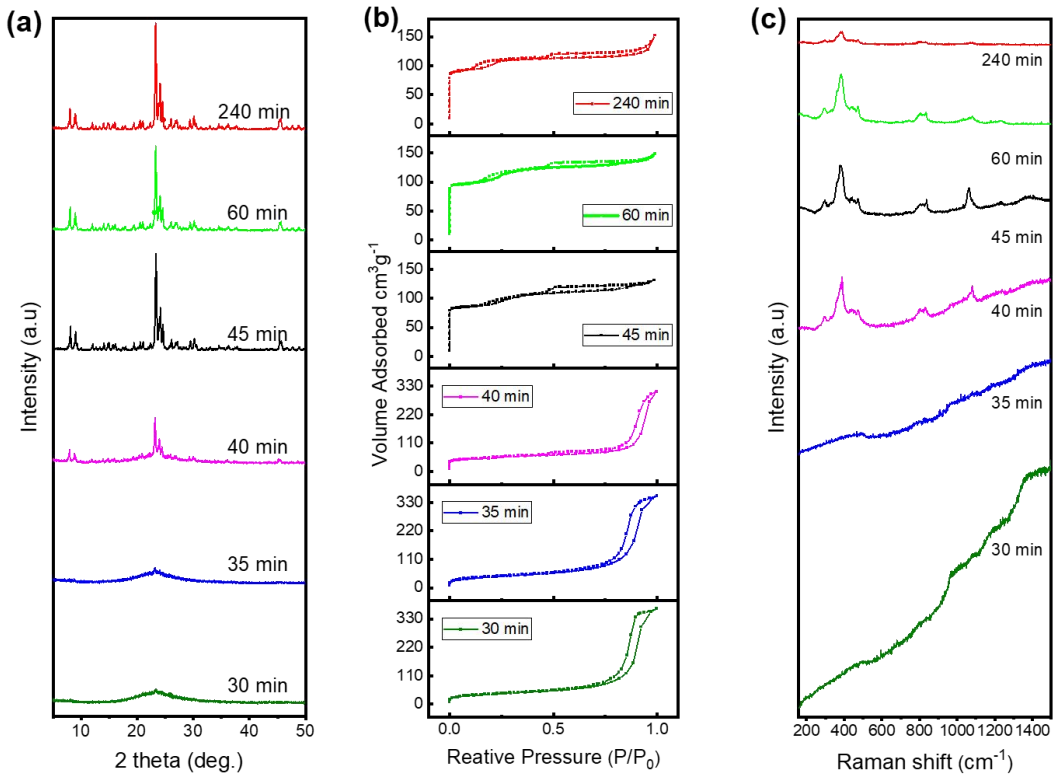


**Figure 3.6.** (a) XRD patterns, (b) $N_2$ adsorption-desorption curve, (c) UV-Raman spectra of as-prepared Silicalite-1 zeolite samples crystallized at different periods at 180 °C, 7 $SiO_2$: 0.5 NaOH: 0.37 TPAOH: 12.5$H_2O$.

The SEM images in Figure 3.7 show as-prepared Silicalite-1 zeolite samples crystallized at different periods. The micrograph structures further support the results shown on gel transformation with time. The powdered reactants shown in Figure 3.7a is the primary amorphous phase of gel transformation.

Figure 3.7b shows SEM images of an increasingly ordered secondary phase of gel transformation. During gel transformation (30-35 min) particles tend to detach and diffuse through the solution as irregular crystals, barely recognizable as an MFI by XRD. Extending the crystallization time to 35 min results in distinct crystals beginning to emerge, although a significant amount of the sample remains amorphous. A further time extension to 40 min shows clear crystal formation with less amorphous material in a process of particle

coarsening. After 45 min of crystallization, spherical uniform crystals can be observed without any amorphous material present, and at this stage, the bulk of the gel reactants are seen to have crystallized. At this crystallization period, perfect and uniform crystals with MFI topology can be observed. A further crystallization time extension to 1 h and 4 h correspondingly transform the crystal phase of the zeolite into unidentifiable bulbous phase structures appearing on the surface of amorphous $SiO_2$. At the same time, amorphous $SiO_2$ begins to disintegrate. In comparison with all the micrographs observed at different periods, 45 min of crystallization time appears to successfully produce pure sub-micron Silicalite-1 with MFI topology at the selected reaction conditions. This is in accordance with earlier suggestions that pure sub-micron Silicalite-1 was rapidly synthesized in 45 min.

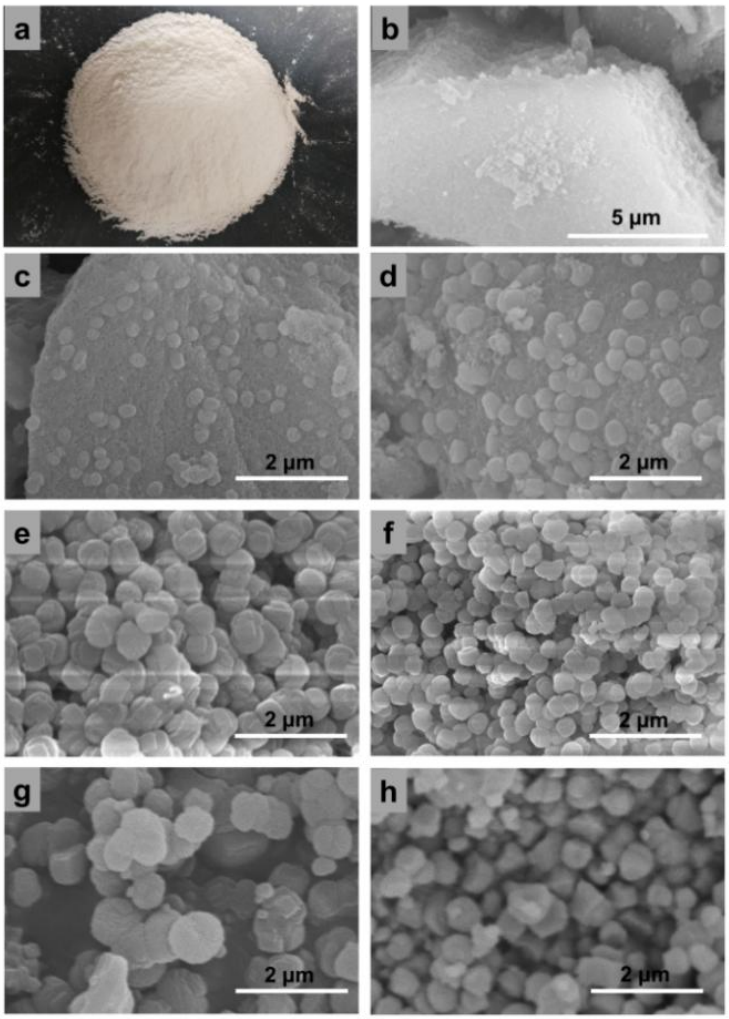

**Figure 3.7.** SEM micrographs of as-prepared Silicalite-1 zeolite samples crystallized at different times, (a) the primary amorphous phase through, (b) the secondary phase (SEM) of equilibrated gel, (c) 30 min, (d) 35 min, (e) 40 min, (f) 45 min, (g) 60 min and (h) 240 min, at 180 °C.

The schematic in Figure 3.8 illustrates the growth mechanism and model of Silicalite-1 zeolite as the homogeneous gel evolves over time from molecular addition to microparticle attachment. The gel transforms into a precipitate phase within 30 min. Between 35 and 45 min, crystallization occurs via propagation and agglomeration in a thermodynamically driven spontaneous process. After 40 min Ostwald ripening occurs where larger particles grow at the expense of smaller particles with simultaneous structural transformations. The mechanism of solvent-free synthesis of Silicalite-1 zeolite is based on the synergy of the classical and non-classical pathways of zeolite precursors being attached to the surface of amorphous $SiO_2$. This is achieved by the extension of crystallization time resulting in the dissolution of amorphous $SiO_2$ structure, restructuring, and three-dimensional growth of Silicalite-1 zeolite crystal. Alexandra et al. used in-situ atomic force microscopy (AFM) to monitor the crystallization growth mechanism of Silicalite-1 and concluded that crystal growth involves a classical mechanism based on the addition of silica molecules and a nonclassical route involving the direct attachment of nanoparticles [15]. It collectively confirms the crystallization phenomenon in Figure 3.7.

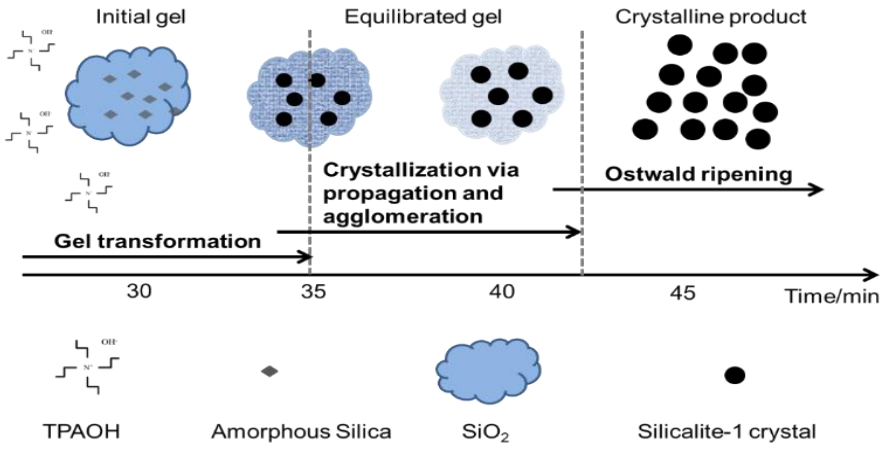


**Figure 3.8.** Rapid gel transformation mechanism of Silicalite-1 zeolite.

## 3.4 Conclusions

In summary, a facile, ultrafast, and low-cost approach was proposed for the synthesis of sub-micron Silicalite-1 with TPAOH organic template. The effect of different amounts of TPAOH on the synthesis procedure was investigated in detail. The synthesis approach was done without the introduction of crystal seeds. The effect of crystallization time and temperature was also studied and the analysis showed that highly crystalline sub-micron Silicalite-1 can be obtained within 45 min at 180 °C. The concept of "green chemistry" designed to reduce or eliminate negative environmental impact was achieved by eradicating the use of solvents and optimizing the amount of TPAOH template used. The crystallization process of sub-micron Silicalite-1 synthesized includes nucleation and crystallization stages. This is a pioneer case where a Silicalite-1 zeolite is rapidly synthesized from raw material under solvent-free conditions, which shows a sustainable approach for the mass production of zeolites. Generally, the solvent-free synthesis strategy used here significantly reduces toxic waste generation and improves efficiency in achieving the production of sub-micron Silicalite-1.

## 3.5. Associated Content

## 3.5.1 Experimental Section

### Zeolites experiment section

### Materials

$NaAlO_2$ (Sinopharm Chemical Reagent Co., Ltd.), NaOH (Shanghai Lingfeng Chemical Reagent Co., Ltd.), Tetrabutylammonium hydroxide (TBAOH, 25%, Shanghai Aladdin Bio-Chem Technology Co., Ltd), $SiO_2$ (Q10, Fuji Silysia Chemical Co., Ltd. Japan), KOH (Sinopharm Chemical Reagent Co., Ltd.), 1,6-

Hexamethylenediamine (Shanghai Macklin Biochemical Co. Ltd.), Commercial HZSM-22 zeolite (Nankai Zeolite Co., Ltd. China). All materials were used without further purification.

## Silicalite-2 zeolite synthesis method

We milled 2.1 g $SiO_2$, 0.1 g NaOH, and 3.2 g TBAOH for 5 min. Then the mixture was added into a 10 mL Teflon reactor and reacted it at 170 $^oC$ for 8 h, then centrifugally washed, dried, and calcined it at 550 $^oC$ for 5 h to get Silicalite-2 zeolite.

## ZSM-22 zeolite synthesis method

During the solvent-free synthesis of ZSM-22, 2.1g $SiO_2$, 0.1 g KOH, 0.1 $NaAlO_2$, 0.1 g HZSM-22 zeolite seed and 2.0 g 1, 6-hexanediamine were added into an agate mortar, respectively, and mechanically ground for 5 min at room temperature to obtain a uniform powder. Then the powder was transferred to a 20 mL Teflon autoclave and heated at 170 $^oC$ for 24 h. The autoclave was quickly cooled to room temperature and filtration was done, succeed by drying at 80 $^oC$, and then the crystalline product of ZSM-22 was obtained.

## Zeolite Characterization

X-Ray Diffraction (XRD) analysis of as-prepared samples was performed on a Rigaku Ultima IV diffractometer with Cu Kα radiation basis and data collected in 2θ = 5-50° (λ=1.54 Å, scanning rate of 5°/min at 40 kV and 40 mA). The morphologies of the synthesized zeolite were investigated with Scanning Electron Microscopy (SEM) and images of all samples were obtained on a Hitachi SU1510. The textural properties of the samples were measured by $N_2$-physisorption on an automatic gas adsorption system (Micromeritics, ASAP 2460). A mass of 0.1 g each sample was used in this process. The samples were previously degassed at 250 °C for 3 h to

remove unwanted gases, organics, and water. The surface area was calculated from the Brunauer-Emmett-Teller (BET) equation whereas the pore sizes were determined by the Barrett-Joyner-Halenda (BJH) method.

## 3.5.2. Results and Characterizations

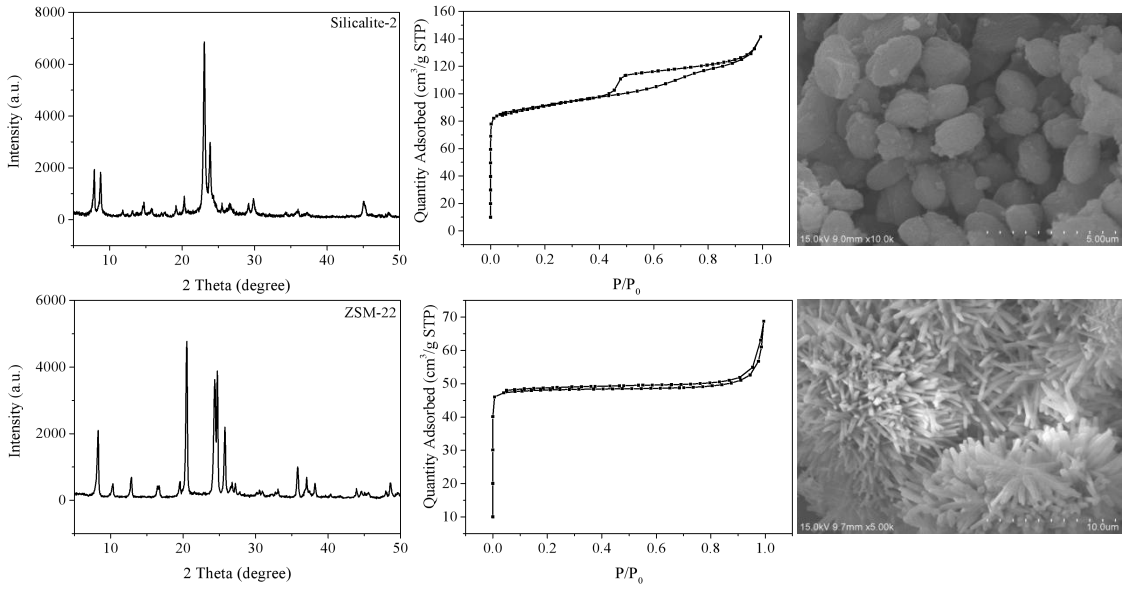


**Figure 3.9.** XRD patterns, $N_2$ adsorption & desorption patterns and SEM micrographs of Silicalite-2, and ZSM-22 zeolites synthesized by solven-free ultrafast synthesis method.

We replaced the template with TBAOH and 1,6-hexamethylenediamine, and successfully prepared Silicalite-2 and ZSM-22 zeolites via same ultrafast synthesis proccess. The XRD spectrum indicates that we have prepared high crystallinity zeolites under a solvent free rapid synthesis route. The $N_2$ adsorption and desorption results indicate that the Silicalite-2 zeolite is mainly characterized by a microporous structure and contains a small amount of mesopores. However, ZSM-22 zeolite only has a microporous structure. The SEM results indicate that the Silicalite-2 zeolite prepared without solvent exhibits an ellipsoid shape with a particle size of approximately 2 μm. ZSM-22 zeolite exhibits a rod-shaped structure with a width of approximately 130 nm.

# References

[1] J. Přech, P. Pizarro, D. Serrano, J. Čejka, *Chem. Soc. Rev.* 47 (2018) 8263-8306.

[2] Z. Han, Y. Shen, F. Wang, X. Zhang, *J. Mater. Sci.* 53 (2018) 12837-12849.

[3] H. Li, Y. Sakamoto, Z. Liu, T. Ohsuna, O. Terasaki, M. Thommes, S. Che, *Micropor. Mesopor. Mat.* 106 (2007) 174-179.

[4] L. Tosheva, V. Valtchev, J. Sterte, *Micropor. Mesopor. Mat.* 35 (2000) 621-629.

[5] W. Wu, D.T. Tran, S. Cheng, Y. Zhang, N. Li, H. Chen, Y.-H.C. Chin, L. Yao, D. Liu, *Micropor. Mesopor. Mat.* 311 (2021) 110710.

[6] A. Deneyer, Q. Ke, J. Devos, M. Dusselier, *Chem. Mater.* 32 (2020) 4884-4919.

[7] D. He, D. Yuan, Z. Song, Y. Tong, Y. Wu, S. Xu, Y. Xu, Z. Liu, *Chem. Commun.* 52 (2016) 12765-12768.

[8] Z. Liu, N. Nomura, D. Nishioka, Y. Hotta, T. Matsuo, K. Oshima, Y. Yanaba, T. Yoshikawa, K. Ohara, S. Kohara, *Chem. Commun.* 51 (2015) 12567-12570.

[9] J. Zhu, Z. Liu, K. Iyoki, C. Anand, K. Yoshida, Y. Sasaki, S. Sukenaga, M. Ando, H. Shibata, T. Okubo, *Chem. Commun.* 53 (2017) 6796-6799.

[10] A. Noreen, M. Li, Y. Fu, C.C. Amoo, J. Wang, E. Maturura, C. Du, R. Yang, C. Xing, J. Sun, *ACS Catal.* 10 (2020) 14186-14194.

[11] F. Pan, X. Lu, T. Wang, Y. Yan, *Mater. Lett.* 196 (2017) 245-247.

[12] T. Iida, M. Sato, C. Numako, A. Nakahira, S. Kohara, T. Okubo, T. Wakihara, *Journal of Materials Chemistry A.* 3 (2015) 6215-6222.

[13] J. Yang, Y.-X. Huang, Y. Pan, J.-X. Mi, *Micropor. Mesopor. Mat.* 303 (2020) 110247.

[14] G. Feng, P. Cheng, W. Yan, M. Boronat, X. Li, J.-H. Su, J. Wang, Y. Li, A. Corma, R. Xu, *Science.* 351 (2016) 1188-1191.

[15] A.I. Lupulescu, J.D. Rimer, *Science.* 344 (2014) 729-732.

[16] C. Zhang, Z. Hong, X. Gu, Z. Zhong, W. Jin, N. Xu, *Ind. Eng. Chem. Res.* 48 (2009) 4293-4299.

[17] A. Maghfirah, M. Ilmi, A. Fajar, G. Kadja, *Materials Today Chemistry.* 17 (2020) 100348.

[18] L. Wang, Y. Xu, G. Zhai, Y. Zheng, J. Huang, D. Sun, Q. Li, *ACS Sustainable Chemistry & Engineering.* 8 (2020) 12177-12186.

[19] I. Díaz, E. Kokkoli, O. Terasaki, M. Tsapatsis, *Chem. Mater.* 16 (2004) 5226-5232.

[20] L. Ren, Q. Guo, H. Zhang, L. Zhu, C. Yang, L. Wang, X. Meng, Z. Feng, C. Li, F.-S. Xiao, *Journal of Materials Chemistry.* 22 (2012) 6564-6567.

[21] X. Deng, Y. Wang, L. Shen, H. Wu, Y. Liu, M. He, *Ind. Eng. Chem. Res.* 52 (2013) 1190-1196.

[22] N. Xu, L. Kong, Y. Zhang, X. Kong, M. Wang, X. Tang, D. Meng, Y. Zhang, *J. Membrane. Sci.* 611 (2020) 118361.

[23] J. Wang, M. Li, Y. Fu, C.C. Amoo, Y. Jiang, R. Yang, X. Sun, C. Xing, E. Maturura, *Micropor. Mesopor. Mat.* 320 (2021) 111073.

[24] M. Liu, H. Wei, B. Li, L. Song, S. Zhao, C. Niu, C. Jia, X. Wang, Y. Wen, *Chem. Eng. J.* 331 (2018) 194-202.

[25] S. Yang, A. Navrotsky, D.J. Wesolowski, J.A. Pople, *Chem. Mater.* 16 (2004) 210-219.

[26] A. Javdani, J. Ahmadpour, F. Yaripour, *Micropor. Mesopor. Mat.* 284 (2019) 443-458.

[27] J. Zhang, H. Ding, Y. Zhang, C. Yu, P. Bai, X. Guo, *Chem. Eng. J.* 335 (2018) 822-830.

[28] X. Meng, F.-S. Xiao, *Chem. Rev.* 114 (2014) 1521-1543.

[29] K. Jiao, X. Xu, Z. Lv, J. Song, M. He, H. Gies, *Micropor. Mesopor. Mat.* 225 (2016) 98-104.

[30] J. Guth, H. Kessler, J. Higel, J. Lamblin, J. Patarin, A. Seive, J. Chezeau, R. Wey, ACS Publications, 1989.

[31] F.C. Pa, A. Chik, AIP Conference Proceedings, AIP Publishing LLC, 2018, pp. 020214.

[32] K. Fukui, T. Nishimoto, M. Takiguchi, H. Yoshida, *Journal of the Society of Powder Technology, Japan.* 40 (2003) 497-504.

[33] H. Liu, Y. Fu, M. Li, J. Wang, A. Noreen, E. Maturura, X. Gao, R. Yang, C.C. Amoo, C. Xing, *Journal of Materials Chemistry A.* 9 (2021) 8663-8673.

[34] C.-H. Cheng, D.F. Shantz, *The Journal of Physical Chemistry B.* 109 (2005) 13912-13920.

[35] S. Tanaka, C. Yuan, Y. Miyake, *Micropor. Mesopor. Mat.* 113 (2008) 418-426.

[36] Q. Wu, X. Wang, G. Qi, Q. Guo, S. Pan, X. Meng, J. Xu, F. Deng, F. Fan, Z. Feng, *J. Am. Chem. Soc.* 136 (2014) 4019-4025.

[37] S. Han, P. Liu, Y. Ma, Q. Wu, X. Meng, F.-S. Xiao, *Ind. Eng. Chem. Res.* 60 (2021) 7167-7173.

[38] L. Ren, Q. Wu, C. Yang, L. Zhu, C. Li, P. Zhang, H. Zhang, X. Meng, F.-S. Xiao, *J. Am. Chem. Soc.* 134 (2012) 15173-15176.

[39] N. Sheng, Y. Chu, S. Xin, Q. Wang, X. Yi, Z. Feng, X. Meng, X. Liu, F. Deng, F.-S. Xiao, *J. Am. Chem. Soc.* 138 (2016) 6171-6176.

[40] J. Deng, S.-F. Sun, E.-Q. Zhu, J. Yang, H.-Y. Yang, D.-W. Wang, M.-G. Ma, Z.-J. Shi, *Ind. Crop. Prod.* 164 (2021) 113412.

[41] S. Al-Khattaf, H. De Lasa, *Ind. Eng. Chem. Res.* 38 (1999) 1350-1356.

[42] M. Lavorgna, L. Sansone, G. Scherillo, R. Gu, A. Baker, *Fuel Cells.* 11 (2011) 801-813.

[43] S. Zeng, R. Wang, Y. Zou, J. Fu, Z. Zhang, S. Qiu, *RSC Adv.* 5 (2015) 95463-95466.

[44] X. Ren, S. Liu, R. Qu, L. Xiao, P. Hu, H. Song, W. Wu, C. Zheng, X. Wu, X. Gao, *Micropor. Mesopor. Mat.* 295 (2020) 109940.

[45] P. Wang, L. Chen, J.-K. Guo, S. Shen, C.-T. Au, S.-F. Yin, *Ind. Eng. Chem. Res.* 58 (2019) 18582-18589.

[46] Z. Xu, H. Ma, Y. Huang, W. Qian, H. Zhang, W. Ying, *ACS omega.* 5 (2020) 24574-24583.

[47] Y. Liu, S. Han, D. Guan, S. Chen, Y. Wu, Y. Yang, N. Jiang, *Micropor. Mesopor. Mat.* 280 (2019) 324-330.

[48] J. Zhang, X. Li, J. Liu, C. Wang, *Catalysts.* 9 (2019) 13.

[49] B. Xie, H. Zhang, C. Yang, S. Liu, L. Ren, L. Zhang, X. Meng, B. Yilmaz, U. Müller, F.-S. Xiao, *Chem. Commun.* 47 (2011) 3945-3947.

[50] B. Xie, J. Song, L. Ren, Y. Ji, J. Li, F.-S. Xiao, *Chem. Mater.* 20 (2008) 4533-4535.

[51] S.-Z. Wang. N.-G. Huang, *PETROLEUM PROCESSING AND PETROCHEMICALS. 30 (1999) 50-55*.

[52] M. Thommes, *Stud. Surf. Sci. Catal.* (2007) 495-523.

[53] B. Mihailova, V. Valtchev, S. Mintova, A.-C. Faust, N. Petkov, T. Bein, *Phys. Chem. Chem. Phys.* 7 (2005) 2756-2763.

[54] J. Zhang, Y. Chu, X. Liu, H. Xu, X. Meng, Z. Feng, F.-S. Xiao, *Chinese Journal of Catalysis.* 40 (2019) 1854-1859.

[55] T. Ikuno, W. Chaikittisilp, Z. Liu, T. Iida, Y. Yanaba, T. Yoshikawa, S. Kohara, T. Wakihara, T. Okubo, *J. Am. Chem. Soc.* 137 (2015) 14533-14544.

# Summary

Energy depletion, greenhouse effect, and industrial waste pollution are the three major world-class challenges that people are facing. Industrialization not only brings people a good life, but also brings these challenges. How to produce green and efficiently has also become an eternal topic for people today. Zeolite materials are widely used in the petrochemical industry as a high-quality catalytic carrier. Especially, it is widely used in the field of C1 chemistry. C1 chemistry can convert $CO_2$ and $H_2$ into high value-added products via zeolite catalysts such as LPG, gasoline, diesel, and alcohols. As a result, people continuously optimize the synthesis process of zeolite to achieve efficient production of zeolite. However, at present, the industrialization of zeolite is still dominated by solvothermal method, that is, high-temperature crystallization production in autoclave with water as solute. Zeolite not only consumes a large amount of energy in this industrial production process, but also generates a large amount of wastewater and safety hazards. Therefore, how to produce zeolite in a green, efficient and safe manner has received widespread attention.

In the chapter 1, we focus on introducing a new method for the synthesis of zeolite under atmospheric pressure using liquid sealing method. The NaA model was used to investigate the effects of crystallization temperature, crystallization duration, type of liquid sealing solution, and quality of liquid sealing solution on the atmospheric pressure crystallization effect of zeolite. At the same time, the characteristic parameters of zeolite synthesized at atmospheric pressure and hydrothermal synthesis were also compared. The results showed that high-quality NaA zeolite was successfully synthesized under the conditions of crystallization at 120 $^{o}$C for four hours and the addition of 30 mg of MC. This also indicates that the liquid sealing method for atmospheric pressure synthesis of zeolite is feasible. Under this method, we further developed the synthesis of other zeolites. FAU zeolite was successfully synthesized by crystallization at 90 $^{o}$C for 18 hours. MFI zeolite was

successfully synthesized by crystallization at 100 °C for 96 hours. BEA zeolite was successfully synthesized by crystallization at 100 °C for 10 days.

In order to further optimize the method of preparing zeolite at atmospheric pressure, we introduced a new method for rapid synthesis of zeolite using a reflux device in the chapter 2. This method conduct atmospheric pressure synthesis of zeolite at higher temperatures which can break the limitations of temperature, small amount of preparation in test tubes, and static crystallization. Due to the presence of reflux devices, solvent loss can be greatly reduced. The results indicate that NaA zeolite can be obtained within four hours at 90 °C. Under this method, we also rapidly synthesized FAU, MFI, and BEA zeolites, repectivily.

In the chapter 3, we developed a solvent-free method for ultra fast synthesis of zeolite. A formula for rapid synthesis of submicron sized Silicalite-1 zeolite was formulated in the $SiO_2$-TPAOH-NaOH system. It was obtained by solid-phase grinding for 5 minutes and crystallization at high temperature for 45 minutes. Due to the absence of solvents, the production process greatly reduces the generation of wastewater. Not only does it greatly reduce energy consumption, but it also reduces the discharge of wastewater. In addition, we can also achieve rapid synthesis of Silicalite-2 and ZSM-22 repectivily by exchanging TPAOH templates with tetrabutylammonium bromide and 1,6-hexanediamine. Silicalite-2 was successfully synthesized at 170 °C for 8 hours. ZSM-22 was successfully synthesized at 170 °C for 24 hours.

These explorations and discoveries provide a new perspective for the green and safe synthesis of new processes for zeolite. Not only has the goal of atmospheric pressure and rapid synthesis of zeolite been achieved, but it also provides a promising path for the green process of zeolite synthesis in the future.

# List of Publications

1. **Xu Sun**, Jiayuan Wang, Yujia Jiang, Elton Maturura, Wenhang Wang, Ruiqin Yang, Chuang Xing, Jiangang Chen, Noritatsu Tsubaki, **Facile synthesis of zeolites under an atmospheric reflux system**, *Microporous and Mesoporous Materials*, 331 (2022) 111646.

2. **Xu. Sun**, Haochen Qi, Yujia Jiang, Qiang Zhao, Peng Lu, Shuyao Chen, Chuang Xing, Elton Maturura, Noritatsu Tsubaki, **Ultrafast green synthesis of sub-micron Silicalite-1 zeolites by a grinding method**, *Journal Of Solid State Chemistry*, 310 (2022) 123016.

3. Yujia Jiang, Haochen Qi, Jiayuan Wang, **Xu Sun**, Changjiang Lyu, Peng. Lu, Ruiqin. Yang, Aqsa Noreen, Chuang Xing, Noritatsu Tsubaki, **Ambient-Pressure Synthesis of Highly Crystallized Zeolite NaA**, *Industrial & Engineering Chemistry Research*, 61 (2022) 1725-1732.

4. Haochen Qi, Chuang Xing, Wenhang Huang, Mingquan Li, Yujia Jiang, **Xu Sun**, Heyang Liu, Peng Lu, Jiangang Chen, Shuyao Chen, **Design of A Hiearchical Co@ZSM-5/SiC Capsule Catalyst For Direct Conversion of Syngas To Middle Olefin**, *Microporous and Mesoporous Materials*, (2022) 112134.

5. Jiayuan Wang, Mingquan Li, Yajie Fu, Cederick Cyril Amoo, Yujia Jiang, Ruiqin Yang, **Xu Sun**, Chuang Xing, Elton Maturura, **An Ambient Pressure Method For Synthesizing NaY Zeolite**, *Microporous and Mesoporous Materials*, 320 (2021) 111073.

# List of Conferences

1. **Xu Sun,** Jiayuan Wang, Mingquan Li, Chuang Xing, Guohui Yang, Noritatsu Tsubaki, **Solvent-free synthesis method of heteroatom zeolite for tuning Fischer-Tropsch synthesis product distribution**, International Chemical Congress of Pacific Basin Societies, Hawaii, America, December 2021, Poster.

2. **Xu Sun**, Yingluo He, Guohui Yang, Noritatsu Tsubaki, **Direct synthesis of gasoline-ranged olefins from syngas over a Na promoted Fe@Na-ZSM-5 capsule catalyst**, The 52nd Petroleum conference, Nagano, Japan, October 2022, Oral (2F 16).

3. **Xu Sun**, Yingluo He, Guohui Yang, Noritatsu Tsubaki, **Construction of a MFI zeolite film catalyst with encapsulated Co partical coated on SiC surface for regulation of Fischer-Tropsch product**, The 4th International Conference on Separation Technology, Johor, Malaysia, Febuary 2023, Oral (ICOST 2023: 025-015).

# Acknowledgements

The three-year doctoral life has come to an end, making it the most difficult one for those who have enrolled for two years in China. Here are many words of gratitude to say.

Firstly, I would like to express my gratitude to my supervisor, Mr. Tsubaki Noritatsu for his academic assistance and guidance. In particular, I would like to thank Mrs Ruiqin Yang and Mr. Chuang Xing from the School of Biology and Chemical Engineering of Zhejiang University of Science and Technology. During the two years of Japan's foreign blockade, it was also the most severe period of the domestic epidemic. Yang 's research group accepted me, who was unable to carry out my doctoral research normally, so that I could complete my thesis and project research normally at Zhejiang University of Science and Technology during my absence from Japan. At the same time, teachers Chengxue Lv, Peng Lu, Xikun Gai, and Shuyao Chen in the group also gave me care in my studies and life. Thank you to Mr Shunli Kou for providing me with the convenience of characterization testing in my doctoral research. I would also like to thank the school leaders of Zhejiang University of Science and Technology for providing me with dormitories and living security for my two-year doctoral research life.

Secondly, I would like to thank my parents for their hard work in raising me from a newborn baby to a PhD during the 30 years of hard work. The kindness of nurturing and nurturing me along the way is indescribable. When I encounter difficulties in my studies and life, my parents are always the first to give me encouragement. Looking back on the road we have traveled, every footprint is filled with their love and education. The years of studying abroad carry the earnest expectations of parents. I would like to express my gratitude to my parents for their selfless support over the years, which has enabled me to pursue my life ideals with such determination.

Then, I would like to thank my friends, who are Wanying Ma, Yandong Song,

Shangyue Li, Guihua Zhang, Yiyang Zheng, Lixin Jiang, Yingnan Cao, and Luping Liu. When I was in Hangzhou for my doctoral research, I was greatly encouraged, supported, and accompanied, allowing me to feel the warmth of home in Hangzhou. I also want to thank Zijian Lu, Yehan Liu, Genhu Ning, Yunhao Cui, and the coaches of Chen Li Gym for finding a happy and healthy body in my boring doctoral life.

Finally, I would like to thank my laboratory classmates for their support and assistance when I encountered difficulties in my research. In particular, I would like to thank my two students, Jiayuan Wang and Yujia Jiang, who are also my research assistant. They have provided the greatest assistance and support on my long research path. Without them, my doctoral research path would be even more difficult. I also wish them all the best in their Master's life.